Clim. Past Discuss., 8, 3277–3343, 2012
www.clim-past-discuss.net/8/3277/2012/
doi:10.5194/cpd-8-3277-2012
© Author(s) 2012. CC Attribution 3.0 License.

Climate of the Past Discussions

This discussion paper is/has been under review for the journal Climate of the Past (CP).
Please refer to the corresponding final paper in CP if available.

Climate and African precipitation changes in the mid-Holocene simulated using an Earth System Model MIROC-ESM

R. Ohgaito[1], T. Sueyoshi[1], A. Abe-Ouchi[2,1], T. Hajima[1], S. Watanabe[1], H.-J. Kim[1], A. Yamamoto[2], and M. Kawamiya[1]

[1]Japan Agency for Marine-Earth Science and Technology, Yokohama, Japan
[2]Atmosphere and Ocean Research Institute, The University of Tokyo, Chiba, Japan

Received: 30 July 2012 – Accepted: 31 July 2012 – Published: 9 August 2012

Correspondence to: R. Ohgaito (ohgaito@jamstec.go.jp)

Published by Copernicus Publications on behalf of the European Geosciences Union.

Abstract

The importance of evaluating models using paleoclimate simulations is becoming more recognized in efforts to improve climate projection. To evaluate an integrated Earth System Model, MIROC-ESM, we performed simulations in time-slice experiments for the mid-Holocene (6000 yr before present, 6 ka) and preindustrial (1850 AD) times under the protocol of the Coupled Model Intercomparison Project 5/Paleoclimate Modelling Intercomparison Project 3. We first overview the simulated global climates by comparing with simulations using a previous version of the MIROC model (MIROC3), which is an atmosphere-ocean coupled general circulation model, and then comprehensively discuss various aspects of climate change with 6 ka forcing. We also discuss the 6 ka African monsoon activity. The 6 ka precipitation change over northern Africa according to MIROC-ESM does not differ dramatically from that obtained with MIROC3, which means that newly developed components such as dynamic vegetation and improvements in the atmospheric processes do not have significant impacts on representing the 6 ka monsoon change suggested by proxy records. Although there is no drastic difference in the African monsoon representation between the two models, there are small but significant differences in the precipitation enhancement in MIROC-ESM, which can be related to the representation of the sea surface temperature rather than the vegetation coupling, at least in MIROC-ESM.

1 Introduction

In efforts to improve climate projection, the importance of evaluating climate models by paleoclimate simulations is being increasingly recognized by the Intergovernmental Panel on Climate Change (IPCC). The Coupled Model Intercomparison Project phase 5 (CMIP5) (Taylor et al., 2009) and Paleoclimate Modelling Intercomparison Project phase 3 (PMIP3) are initiatives for the evaluation of models endorsed by the

CPD
8, 3277–3343, 2012

World Climate Research Programme and the International Geosphere-Biosphere Programme.

CMIP5/PMIP3 proposes several coordinated paleoclimate simulations to evaluate the different model outputs against paleoproxy records (Braconnot et al., 2012). The mid-Holocene (6000 yr before present; hereafter, 6 ka) has been used as a benchmarking period. The period 6 ka is characterized by enhanced seasonality in the Northern Hemisphere and reduced seasonality in the Southern Hemisphere due to a difference in solar insolation compared with the present day, associated with orbital variations of the Earth (Berger, 1978). Many proxy records such as pollen (Prentice et al., 2000; Harrison et al., 2001; Bigelow et al., 2003; Pickett et al., 2004; Wohlfahrt et al., 2008; Bartlein et al., 2011) and lake status data (Kohfeld and Harrison, 2000; Yu et al., 2000; Harrison et al., 2003; Lezine et al., 2011) suggest humid and vegetated conditions over the Sahara desert.

Paleoclimate Modelling Intercomparison Project phase 1 (PMIP1) compared simulations using atmospheric general circulation models (AGCMs) and reported the enhancement and northward shift of the summer African and Indian monsoons in 6 ka (Joussaume et al., 1999). The modeled climate changes were consistent in sign with paleoclimate proxy records, but failed to simulate an increase in precipitation sufficient to maintain a fully vegetated Sahara.

Models with various levels of complexity have been used to investigate the effect of vegetation feedback to the African monsoon change in 6 ka. Using an intermediate complexity model, Ganopolski et al. (1998) found that vegetation played a role in the increase in subtropical precipitation. There have been several attempts to simulate vegetation and/or ocean feedback using an asynchronous coupling scheme. Texier et al. (1997) simulated a 2.5-degree northward shift of vegetation in the Sahara. Claussen (1997) showed the possibility of a multiequilibrium vegetation state. Braconnot et al. (1999) coupled vegetation (diagnoses) and an oceanic general circulation model (OGCM) asynchronously to an AGCM and concluded that both contribute to enhance African precipitation. An alternative way to test the vegetation feedback to

CPD
8, 3277–3343, 2012

monsoon activity around 6 ka is to simulate the situation at that time using a boundary condition derived from the vegetation type reconstructed from pollen proxy records (Kutzbach et al., 1996b; Brostrom et al., 1998; Knorr and Schnitzler, 2006). Such studies reported that paleovegetation provides a positive feedback to the monsoon, but the precipitation enhancement was insufficient to maintain vegetation. Full coupling of the different climatic components was first implemented around the beginning of the 21st century. A study employing atmosphere-vegetation coupling revealed more grassland at the desert border (Doherty et al., 2000). Levis et al. (2004) carried out atmosphere-ocean-vegetation coupled simulations and concluded that the albedo change is important to increased precipitation. However, one model indicated negative vegetation-precipitation feedback (Notaro et al., 2008; Wang et al., 2008), although it has been reported that the feedback is dependent on the vegetation type (Liu et al., 2010).

In addition to the low-latitude changes, Kutzbach et al. (1996a) claimed that the lowering albedo in the northern high latitudes, suggesting expansion of vegetation, facilitates the northward expansion of vegetation. Although Otto et al. (2009) reported that the contribution of vegetation to warming at northern high latitudes is small compared with the contributions of the atmosphere and ocean, O'ishi and Abe-Ouchi (2011) claimed that a dynamic vegetation model provided a larger positive feedback to 6 ka climate temperature changes over Siberia.

We now consider studies reporting the role of the ocean in the African and Asian monsoons. Hewitt and Mitchell (1998) compared experimental results obtained using an atmosphere-ocean coupled general circulation model (AOGCM) and an AGCM under 6 ka insolation forcing. The ocean coupling enhanced precipitation over Africa, India, and the Indian Ocean. Braconnot et al. (2000) reported that the African and Asian monsoons were enhanced with ocean coupling. On the other hand, Voss and Mikolajewicz (2001) reported that monsoon enhancement was suppressed with ocean coupling in Asia. Their results were based on long-term integrations of AGCM simulations periodically coupled with an OGCM. Using asynchronous coupling of an AGCM

CPD
8, 3277–3343, 2012

and OGCM, Liu et al. (1999) reported that the Asian monsoon was attenuated with ocean coupling according to analyses of the monsoon response to 11 ka orbital forcing. Liu et al. (2003) carried out AOGCM simulations for several Holocene time slices and found that ocean coupling attenuated the Asian monsoon enhancement. Dallmeyer et al. (2010) used an Earth system model (ESM) and investigated the effect of vegetation and ocean components on the total change to the Asian monsoon in 6 ka. They found that the ocean played a major role in the monsoon change.

Zhao et al. (2005, 2007) and Zhao and Harrison (2011) made a multimodel intercomparison and reported that the sea surface temperature (SST) pattern played a role in the enhancement of the African monsoon. Ohgaito and Abe-Ouchi (2007) reported that ocean thermodynamics played a major role in the further enhancement of the African monsoon and attenuation of the Asian monsoon. The consistent results were reported by Marzin and Braconnot (2009a, b). Ohgaito and Abe-Ouchi (2009) reported the importance of the present-day SST reproduction to Asian monsoon changes in 6 ka.

Although the present work focuses on climate and monsoon changes in 6 ka, the mechanisms responsible for the present-day monsoon variability suggest how to investigate what happens to the monsoon area under the situation of climate change. We briefly look at the types of influence that have been reported in studies on the strength of the modern African monsoon. Many studies on the variability of present-day Sahel precipitation suggest correlation with the ocean. Ocean forcing is the dominant driver of the decadal West African monsoon variability (Biasutti et al., 2008).

The influence of the SST variability on the African monsoon is intensively investigated as part of the African Monsoon Multidisciplinary Analyses project. The SST in each basin, such as the Mediterranean Sea, Indian Ocean, and Atlantic Ocean, affects the interannual variability of the monsoon, whereas the global pattern affects the decadal variability of the monsoon (Rodriguez-Fonseca et al., 2011; Mohino et al., 2011; Losada et al., 2010a, b). Fontaine et al. (2010) suggested that a warm Mediterranean SST leads to a strong West African monsoon. On the other hand, Bader and Latif (2003) suggested that a warm Indian Ocean SST correlates to less Sahel

CPD
8, 3277–3343, 2012

precipitation. Vizy and Cook (2001) stated that the SST over the Gulf of Guinea and eastern North Atlantic affects the African monsoon.

There are many works on present-day soil moisture-monsoon feedback (Xue et al., 2004; Douville et al., 2001, 2007; Bergengren et al., 2001; Philippon et al., 2005) suggesting that the enhanced soil moisture favors a strong monsoon. There have been few studies on the present-day vegetation-monsoon feedback, but Zeng et al. (1999) showed that vegetation amplifies monsoon activity. To understand the mechanisms responsible for monsoon changes under the situation of climate change, it is necessary to consider the roles played by these factors.

Besides discussing precipitation variation and its causes, Wang et al. (2011) proposed the idea of the global monsoon (GM). Monsoon rainfall is an essential feature of the seasonal contrast of the Earth's hydrological cycle. The concept of the GM has proven to be a useful tool in investigating the trend (Wang and Ding, 2006; Wang et al., 2011) and interannual variability (Kim et al., 2011) of the hydrological cycle, and to examine a numerical model's fidelity (Wang et al., 2011). The GM concept will be applied to evaluate monsoon changes in 6 ka in Sect. 5.

For future climate projection and for climate-change studies, the importance of the carbon cycle in the environment has been recognized in IPCC reports. The MIROC team developed an ESM, namely MIROC-ESM (Watanabe et al., 2011). The newly developed model should be tested against various conditions to instill confidence in climate projection using the model. Paleoclimate experiments provide a unique opportunity for such testing. To evaluate MIROC-ESM, we performed simulations of time slice experiments for 6 ka (corresponding to mid-Holocene (exp3.4) in the CMIP5 database) and 0 ka (corresponding to piControl (exp3.1) in the CMIP5 database) under the CMIP5/PMIP3 protocol as described by Sueyoshi et al. (submitted).

In this study, we overview the climate changes simulated using MIROC-ESM under 6 ka forcing. Furthermore, we focus on the African monsoon activities in 6 ka. We present various analyses in which the MIROC-ESM results for African precipitation are compared with results obtained with MIROC3, which is a previous MIROC AOGCM,

CPD
8, 3277–3343, 2012

and discuss possible factors affecting the representation of monsoon changes in 6 ka. It is worth comparing the two similar models MIROC-ESM and MIROC3, for which we know the difference in components, and discussing the consistency and differences of the represented climate change to explore the source of the difference in climate-change simulation.

This work is organized as follows. We firstly explain the model and experimental setup in Sect. 2. A 0 ka climate representation is then shown in Sect. 3. The global changes in 6 ka are explained in Sect. 4 followed by analyses of monsoon changes in 6 ka in Sect. 5. Finally, we conclude the work in Sect. 6.

2 Models and experimental setup

2.1 Model description

We use three models in this work, namely the ESM, MIROC-ESM, and AOGCM MIROC3, and the AGCM part of MIROC3 for additional sensitivity experiments. Because MIROC-ESM is based on MIROC3, we firstly explain MIROC3 briefly, and then the differences in MIROC-ESM.

MIROC3 is an AOGCM; the MIROC3.2 (medium resolution) (K-1 model developers, 2004) which was used in the IPCC Fourth Assessment Report (AR4). The AGCM part has a horizontal resolution of spectral T42 and 20 vertical layers (the top of the atmosphere is at 10 hPa) and is coupled with the land module MATSIRO in which the leaf-area index (LAI) is prescribed. The biogeochemical cycle is not included. The vegetation types are prescribed to have modern distributions for the experiments in this work. The OGCM module has a resolution of about horizontal 1° and 44 vertical layers. The model has a simplified aerosol transportation component sSPRIANTARS.

MIROC-ESM was developed to better simulate future climate projection (Watanabe et al., 2011). It has components of an AGCM with a horizontal atmospheric resolution of T42 and 80 vertical layers including the stratosphere coupled with the land

CPD
8, 3277–3343, 2012

module MATSIRO, and an OGCM part that is identical to that for MIROC3. MIROC-ESM has an aerosol transportation model SPRINTARS (Takemura et al., 2000, 2002, 2005), a terrestrial ecosystem component called the Spatially Explicit Individual-Based Dynamic Global Vegetation Model (SEIB-DGVM) (Sato et al., 2007), an ocean ecosystem component, and improved radiation code "mstrmX", which eliminates the cold bias (Sekiguchi and Nakajima, 2009) in the previous version of MIROC (MIROC3). The chemistry module CHASER is not activated in our experiments.

The newly incorporated component for MIROC-ESM, SEIB-DGVM, calculates vegetation dynamics such as photosynthesis, respiration, growth, and mortality. There are 17 vegetation types as listed in Table 2. The component predicts the LAI during the calculation. The above processes are computed using physical variables calculated by MIROC-ESM. The LAI is then given for the calculations of biogeophysical processes in MATSIRO: the processes for radiation transfer including surface albedo, interception of precipitation, and energy transfer through latent and sensible heat. The carbon cycle is fully calculated for the atmosphere, land, and ocean. The two models are compared in Table 1. The model structures were schematically presented by Sueyoshi et al. (2012). Additionally, several sensitivity experiments are performed using the AGCM part of MIROC3. Details are given in Sect. 2.2.

2.2 Experimental setup

We performed sets of simulations in time-slice experiments for 6 ka and 0 ka under the CMIP5/PMIP3 protocol. The major difference between 0 ka and 6 ka conditions was the Earth's orbit. Additionally, there was a small difference in the greenhouse-gas levels. The other boundary conditions were the same. The orbital parameters for 6 ka were set as eccentricity of 0.018682, obliquity of 24.105°, and perihelion of 180.87° (Berger, 1978). As the greenhouse gases, CO_2, N_2O, and CH_4 had 6 ka concentrations of 280, 0.27, and 0.65 ppm, respectively. In the 0 ka experiment, the orbital parameters were 0.0672, 23.45°, and 102.04° for the eccentricity, obliquity, and perihelion, respectively. Because the experiments using MIROC3 were performed earlier than CMIP5, there is

CPD
8, 3277–3343, 2012

a little difference between greenhouse gases for 0 ka for MIROC-ESM and MIROC3. CO_2 and N_2O levels are the same for the two models (285 ppm and 0.28 ppm) but CH_4 levels are 0.79 ppm and 0.86 ppm for MIROC-ESM and MIROC3, respectively. The effect of this greenhouse gas difference is more than one order smaller than that of the difference of the forcing of 0 ka and 6 ka (not shown).

The change in solar insolation at the top of the atmosphere in 6 ka compared with that in 0 ka is plotted in Fig. 1. In 6 ka, seasonality was enhanced in the Northern Hemisphere and weakened in the Southern Hemisphere, especially at mid-latitudes. There was more annual net solar radiation at high latitudes and less in the tropics, compared with the case in 0 ka.

The 0 ka simulation using MIROC-ESM was integrated for 629 years, and the climatology of the last 100 yr was used for the analyses. The 6 ka simulation using MIROC-ESM was initiated from the 250th year of the 0 ka simulation and integrated for 379 yr, and the climatology for the last 100 years was used for the analyses. In MIROC3 simulation, the 0 ka experiment was integrated for 1050 yr and the climatology of the last 100 yr was used for the analyses; this analysis is referred to as M30ka or 0 ka for MIROC3. The 6 ka experiment was integrated for 650 yr, and the climatology of the last 100 yr was used for the analyses; this analysis is referred to as M36ka or 6 ka for MIROC3. These experiments are identical to those carried out by Ohgaito and Abe-Ouchi (2007) and submitted to PMIP phase 2 (PMIP2). The experimental setup is schematically illustrated in Fig. 2, and the experiments are listed in Table 3.

We performed additional sensitivity experiments using the AGCM part of MIROC3 to deepen the understanding of the precipitation changes over the Sahara Desert in 6 ka. The reason for basing the tests on MIROC3 is that MIROC-ESM has a cost one order of magnitude higher than that of MIROC3. The sensitivity experiments are listed in Table 4. M3Amiroc3 is the experiment sets (0 ka and 6 ka) of the MIROC3 AGCM with prescribed SSTs, which are the climatologies of the MIROC3 experiments for 0 ka and 6 ka. M3Aesm is the same as M3Amiroc3 but with SSTs simulated in MIROC-ESM. M3Aesmofs is an additional 6 ka experiment associated with M3Aesm. The SST in the

CPD
8, 3277–3343, 2012

6 ka experiment of M3Aesmofs is the climatological SST simulated using MIROC-ESM but the global level is offset by +0.4 °C to check if global cooling might have affected precipitation enhancement over the Sahara.

M3Alai is another test for the vegetation feedback. The climatological LAI obtained in 0 ka and 6 ka simulations using MIROC-ESM were used in MIROC3 AGCM experiments as boundary conditions instead of the observation-based LAI, which is prescribed in M3Amiroc3. The SSTs are the same as for M3Amiroc3. All the sensitivity experiments were integrated for more than 20 yr, and climatologies for more than 15 yr were used in the analyses.

3 0 ka climate representations

3.1 Atmospheric variables

The simulated 0 ka basic climatic variables were compared with observation-based reanalysis data (not shown). The temperature distribution is in good agreement with the European Centre for Medium-Range Weather Forecasts reanalysis (ERA-40) data both for MIROC-ESM and MIROC3. Slight cooling in the 0 ka simulations arises from differences in the greenhouse-gas levels for the preindustrial era and those in the 20th century. The precipitation distributions suggest that the South Pacific Convergence Zone obtained with the two models is somewhat weaker than that described by the reanalysis data, but the Inter Tropical Convergence Zone (ITCZ) of the models is reasonably reproduced. Overestimation of the precipitation amount over the Northern African and Asian monsoon areas using MIROC3 is improved using MIROC-ESM. Watanabe et al. (2011) performed a 20th century transient experiment using MIROC-ESM, and obtained reasonable decadal global averaged temperature rises and falls when compared with observational data.

CPD
8, 3277–3343, 2012

3.2 Oceanic variables

Net SST biases relative to the World Ocean Atlas 1998 (World Ocean Atlas, 1998) are plotted in Fig. 3. Although the bias is more significant over the Pacific Ocean for MIROC-ESM, with cooler tropics and warm high latitudes, both the models reasonably simulate the global SSTs. Note that generally negative biases are expected because of a difference between the time of the experimental 0 ka (1850 AD) and that of the observations in the 20th century.

The sea-surface salinity was also compared with data from the World Ocean Atlas 1998 (data not shown). The models well reproduce the global distribution, such as the saline area over mid-latitudes, salinity contrast between the Atlantic Ocean and Pacific Ocean, and fresh water over the Arctic Sea and the Warm Pool.

3.3 Distribution of carbon in MIROC-ESM

It is possible to calculate the carbon amounts in the atmosphere, ocean, soil, and vegetation in MIROC-ESM. The amounts in 0 ka were 6.1×10^2 GtC (gigatonne of carbon) in the atmosphere, 3.6×10^4 GtC in the ocean, 2.5×10^3 GtC in soil, 4.7×10^2 GtC in vegetation, and 3.1×10 GtC in land used by humans. Each amount appears reasonable when compared with values presented in Chapter 7 of IPCC AR4 (Sarmiento and Gruber, 2006), specifically 38 000 GtC in the ocean, 600 GtC in the atmosphere, and 2300 GtC in the soil, vegetation, and detritus. The carbon amounts were calculated but the CO_2 level used for the atmospheric calculations was not modified in the simulations following the PMIP3/CMIP5 protocol.

CPD
8, 3277–3343, 2012

4 Global changes in 6 ka

4.1 Atmospheric changes in 6 ka

The 6–0 ka temperature changes are compared in Fig. 4 for June–September (JJAS) and December–February (DJF). We analyze JJAS and not June–August to capture the prolonged boreal summer under the 6 ka forcing, as many previous works on 6 ka have done. Both MIROC-ESM and MIROC3 show warming over most of the boreal continents following 6 ka insolation change in JJAS. The less warming over North America in MIROC-ESM is more consistent with what the archive of proxy records suggests (Bartlein et al., 2011). The two models show slight cooling over the tropical ocean and the African and Asian monsoon regions, which would be caused by strengthened monsoon activities. The Southern Ocean in JJAS is cooled more in MIROC-ESM. If the temperature responded simply to the radiation change in 6 ka, it would fall. In DJF, most of the continents became cooler following the insolation change in 6 ka. MIROC-ESM indicates greater cooling than MIROC3. Hovmoller diagrams in Fig. 5 depict cooling during the boreal winter and warming in the boreal summer for both models. Both models simulate slightly lower net temperature changes for 6 ka but MIROC-ESM (−0.65 °C) simulated a larger temperature drop than did MIROC3 (−0.26 °C). This must be due to differences in AGCM components (e.g. cloud, aerosols and so on) and/or vegetation between the two models. However, the difference is too small to judge which model presents the more appropriate change by the proxy recoreds.

Changes in the meridional heat transport in 6 ka are shown in Fig. 6. Both models simulate generally similar changes. The ocean transports more heat northward over the tropics. The net poleward heat transport in both hemispheres is reduced mainly by changes in atmospheric heat transport, which is consistent with the reduced meridional radiation gradient.

The global atmospheric circulation is also affected. Figure 7 illustrates the 6–0 ka velocity potential changes as deviations from the zonal mean, which suggest a change in Walker circulation. MIROC-ESM and MIROC3 show generally consistent changes

CPD
8, 3277–3343, 2012

to Walker circulation. The JJAS divergences from India to Southeast Asia are greater and shifted westward in 6 ka. The changes are most pronounced over northern Africa. Peak latitudes of precipitation for 6 ka and 0 ka are also plotted. The area of pronounced northward shift of the peak latitudes in JJAS in 6 ka corresponds to the central area of the velocity potential changes. These circulation changes are consistent with the African and Asian monsoon enhancements. The convergences also strengthened and shifted westward over the Pacific Ocean. The 6 ka changes in DJF also suggest strengthening of the circulations but the strengthened divergence changes are mainly over the Indian Ocean.

The global distributions of the precipitation changes in 6 ka are plotted in Fig. 8 for JJAS and DJF. We see a general resemblance of the precipitation changes in 6 ka obtained by MIROC-ESM and MIROC3. In JJAS, an enhanced-precipitation belt from the equator to the Sahel regions over the African continent is seen for the two models. The details are discussed in Sect. 5. Additionally, there is common enhanced precipitation over northern India accompanied with weakened precipitation over southern India. The ITCZ shifts northward over the Atlantic Ocean, whereas it does not change position and weakens over the Pacific Ocean (Figs. 7 and 8). In DJF, there is enhanced precipitation over the Indian Ocean and reduced precipitation over the continents and over the western tropical Pacific, suggesting weakened monsoon activity for both models. The ITCZ shifts southward over the Atlantic Ocean (Fig. 7).

Associated with precipitation changes in 6 ka, soil moisture changes are shown in Fig. 9. The two models reveal enhanced soil moisture over northern Africa, covering the Sahara Desert, and northern India, and reduced soil moisture over most of Eurasia and North America. The 6 ka changes over Africa, India, and North America are consistent with proxy records of lake status (Kohfeld and Harrison, 2000; Yu et al., 2001; Harrison et al., 2003). In particular, over Africa, not only moistening over the Sahara but also moistening over the tropical coastal area of Eastern African is reproduced by the models.

CPD
8, 3277–3343, 2012

4.2 Oceanic changes in 6 ka

SST changes obtained using the two models for JJAS and DJF in 6 ka are shown in Fig. 10. Tropical cooling almost throughout the year and warming at northern high latitudes in JJAS are consistent for the two models. MIROC-ESM shows slightly cooler SST changes. MIROC-ESM simulates cooling whereas MIROC3 simulates warming in the northern Atlantic Ocean. The JJAS cooling is unexpected from the 6 ka radiation change at northern mid/high latitudes. Figure 11 presents the seasonal evolution of the SST change in 6 ka over the northern Atlantic Ocean and the radiation changes. The SSTs suggest reasonable seasonal evolution following the radiation change but there is an offset of about −0.5 °C for MIROC-ESM compared with MIROC3. As a result, the JJAS change becomes negative. The cooler change compared with the change obtained with MIROC3 is due to differences in the surface radiation budget. The longwave radiation changes in 6 ka are about 3 W m^{-2} less than those obtained with MIROC3 throughout the year. Additionally, the change in shortwave radiation suggests weaker enhancement during the boreal summer associated with the enhancement of low-level cloud cover over this area. These differences in the 6 ka and 0 ka surface radiation changes lead to lower SST during the winter and a hardly positive SST change during the following summer.

In DJF, as in JJAS, the results obtained with MIROC-ESM are generally slightly cooler than those obtained with MIROC3. The degree of cooling is higher for MIROC-ESM, especially over northern high latitudes. The pattern of cooling is similar for MIROC-ESM and MIROC3. The Southern Ocean is warmed according to MIROC3 whereas it is cooled according to MIROC-ESM as in the temperature change. Although there are differences between the two models in the ocean responses, the SST changes in 6 ka are almost within ± 1 °C. We are unable to state which model is better than the other by the proxy records. What we can say is that the difference between the models is due to differences in the atmosphere and land modules because the OGCM parts of the two models are identical.

CPD
8, 3277–3343, 2012

Figure 12 depicts the oceanic surface stream function and changes in 6 ka for the Pacific and Atlantic basins in the Northern Hemisphere. The changes in the strength of the Kuroshio in 6 ka are less than 1 Sv for both models. On the other hand, the Atlantic changes have different amplitudes for the two models, though the patterns of change are common. MIROC3 simulates a strengthening of more than 5 Sv for the Gulf Stream in 6 ka, whereas MIROC-ESM simulates a change of 1 Sv. This heat transport change may also support the difference in the changes in the North Atlantic temperature between the two models. The difference in subtropical gyre responses between the two models can be attributed to the surface wind stress differences because the oceanic parts of the two models are identical. The net enhancement of the surface wind stress is about 0.01 $\mathrm{N\,m^{-2}}$ along the direction of the Gulf Stream for MIROC3 over the area of the strengthened Gulf Stream, whereas MIROC-ESM simulates no large change in the surface stress in 6 ka. The surface wind stress change in 6 ka would be partly due to the difference in the warming level over the North American continent, which must be a result of the differences in the atmosphere and land processes between the two models.

The sea ice expansions and convection sites in the Northern Hemisphere in 0 ka are reasonably reproduced by the two models (data not shown). However, in the Southern Hemisphere, the sea ice extents obtained with the two models are smaller than the boundary condition of Atmospheric Model Intercomparison Project II (Hurrell et al., 2008), which results from the warm SST bias indicated in Fig. 3.

The sea ice extents do not change drastically in 0 ka and 6 ka according to the two models probably because of the weak radiation forcing. However, associated with the Southern Ocean cooling in MIROC-ESM, there is a greater extent of sea ice around Antarctica in 6 ka. In the Northern Hemisphere, associated with the northern warming in the boreal summer, the summer sea ice extents in 6 ka are reduced according to the two models. Changes in winter in 6 ka are small (data not shown).

Annual changes in sea surface salinity in 6 ka are generally less than 1 PSU (data not shown) and the patterns of the changes are consistent between the two models.

CPD
8, 3277–3343, 2012

Freshening over the Indian Ocean and more saline changes around the Warm Pool are commonly seen. These changes are due to changes in net precipitation minus evaporation and oceanic circulation changes (Fig. 12).

Concerning thermohaline circulation, neither model indicated a large change in the Atlantic Meridional Overturning Circulation in 6 ka. The peak values are 17.0 Sv for 0 ka and 17.7 Sv for 6 ka in MIROC-ESM, and 19.2 Sv and 20.5 Sv for 0 ka and 6 ka in MIROC3. Therefore, the thermohaline circulation would have little effect on 6 ka climate change.

4.3 Vegetation responses in MIROC-ESM

In MIROC-ESM, coupling between MATSIRO and SEIB-DGVM is relatively loose owing to the structural discrepancies between the two modules, and some ecological changes predicted in the terrestrial ecosystem module are not reflected in MATSIRO (e.g. changes in plant functional type composition and its spatial pattern modify the terrestrial biogeochemical processes but do not affect physical land processes except for those associated with the LAI). However, it is worth checking such internally predicted ecological information in SEIB-DGVM, because it demonstrates the potential of MIROC-ESM to reproduce vegetation feedback to the climate inputs from the AGCM part of MIROC-ESM. Figure 13 plots the most frequent vegetation types in 0 ka and 6 ka MIROC-ESM simulations. The grids where the vegetation types flip-flop (i.e. there is no dominant vegetation type – > 50 %) are white. Over the Sahel region, the grasslands shift about 1 grid northward and the tropical rainforest expands northward in 6 ka. Although the most frequent vegetation types do not shift by more than one grid, permanent desert reduces significantly (Fig. 14). Such sporadic vegetation coverage over much of the Sahara may leave pollen proxy records.

The boundary of tundra grassland over Siberia shifts about 1 grid northward which is associated with the warming. This is consistent with what has reported by Bigelow et al. (2003) and O'ishi and Abe-Ouchi (2011). The forest types at mid-latitudes to high latitudes in Eurasia also generally shift northward.

CPD
8, 3277–3343, 2012

4.4 Carbon redistribution simulated with MIROC-ESM

Carbon amounts are 2.4×10^3 GtC for soil, 5.3×10^2 GtC for vegetation, 3.6×10^4 GtC for the ocean, and 5.6×10^2 GtC for the atmosphere in the 6 ka MIROC-ESM simulation. Compared with 0 ka, there is a redistribution of carbon in the system. There is no significant change in the carbon amount in the ocean. The atmospheric carbon is 9 % less, the carbon stored in vegetation is 12 % greater, and the carbon stored in soil is about 4 % less in 6 ka. This redistribution could be due to the active vegetation in 6 ka. Note that the CO_2 concentration in the atmosphere is prescribed in both 0 ka/6 ka simulations and there is therefore no feedback of the change in the carbon cycle to the simulated physical field.

5 Summer monsoon changes in 6 ka

5.1 Overview of global summer monsoon changes in 6 ka

Associated with the ITCZ changes in 6 ka explained in Sect. 4.2., the Asian and northern African monsoon activities in the Northern Hemisphere summer are enhanced in 6 ka in both MIROC models (Fig. 8). Sea-level pressure changes (Fig. 15) in 6 ka suggest lower air pressure over the continents in JJAS, which is consistent with the enhancement of the summer monsoon. The two models reveal generally consistent changes in 6 ka.

Figure 16 presents the GM domain and global monsoon precipitation index (GMPI, a ratio of local summer rainfall to annual total, Wang et al., 2011). Both the MIROC-ESM and MIROC3 simulations for the 0 ka climate generally capture reasonably well the various monsoon systems around the globe (Fig. 16a and d). However, the GMPI over the Western Sahara obtained with MIROC3 seems too high when compared with the observed GMPI (Kim et al., 2011). The regional monsoons bear close resemblance to the pluvial maxima derived from the 6 ka simulations (Fig. 16b and e). However,

CPD
8, 3277–3343, 2012

it is evident that the northern limit of the northern African monsoon extends farther northward in association with the enhanced GMPI (Fig. 16c and f). Indeed, the areal extent of the GM domain generally varies in tandem with the change in the rainfall seasonality; the expansion (retreat) tends to coincide with the amplified (reduced) local summer rainfall.

The GMPI in northern African regions including the Sahara and the Arabian Peninsula, and the northern edge of the monsoon domain is higher in 6 ka. MIROC-ESM shows that the enhancement of the GMPI widely covers the Sahara whereas MIROC3 shows that the enhancement is limited to the eastern Sahara region. This could be related to the difference in the GMPI representations for 0 ka.

Although GM domains hardly change in 6 ka, the austral summer monsoons are generally weaker. Additionally, both models reveal a decrease in precipitation over the Southern Hemisphere continents in DJF in 6 ka (Fig. 8b and d). This is consistent with the 6 ka orbital forcing (Fig. 1) and also the results of a previous work (Liu et al., 2004).

No large 6 ka changes are observed in the North American monsoons according to the two models. Major changes are seen for the northern African and Asian monsoons. In the following subsections, we focus on the northern African and Asian monsoons, and we refer to the former as the African monsoon.

5.2 Asian and African monsoons

The low-tropospheric wind and precipitation changes in JJAS for the African and Asian monsoons in 6 ka are depicted in Fig. 17. The two models simulate a northward shift of precipitation over Africa and Asia. The circulation changes also indicate enhanced monsoon circulation in 6 ka. MIROC-ESM indicates slightly greater precipitation over the Sahara than MIROC3, which is also illustrated in Fig. 16c and f. The convective activities shift northward in the Sahel and Sahara regions according to the two models (Fig. 18). In Fig. 18, the strength of convection changes at a height of 500 hPa in 6 ka are plotted for the two models, and the results suggest enhancement and northward expansion of the convective activities. The difference between the two models is small

CPD
8, 3277–3343, 2012

but most pronounced in early summer. Seasonal evolution of the precipitation changes compared with 0 ka for the African area (20° W–30° E, 8–24° N) and Asian area (70–140° E, 22–40° N) are compared in Fig. 19 for MIROC-ESM and MIROC3. The 6 ka precipitation changes for MIROC-ESM and MIROC3 suggest similar seasonal evolution but the onset of the African monsoon obtained with MIROC-ESM seems a little earlier than that obtained with MIROC3, and the peak enhancement in the Asian region is higher for MIROC-ESM than for MIROC3. To investigate in more detail, we plot the Hovmoller diagrams of the 6 ka precipitation changes for the African and Asian areas (Fig. 20). The 0 ka precipitation is plotted with black contours. The two models simulate similar seasonal precipitation evolutions. For the African area, there is a northward shift of summer precipitation, with reduced precipitation in winter to spring. In MIROC-ESM, the precipitation covers the Sahara during early summer in 6 ka. The level of enhancement is insufficient to maintain vegetation over the Sahara; however, the enhancement is significant. This is discussed further in the following subsections. For the Asian area, both models simulate a northward shift of precipitation in summer, accompanied with a reduction in precipitation to the south. Figure 21 shows the 6 ka low-tropospheric zonal wind changes over the African and South Asian regions as determined by the two models. Both models indicate an enhancement and northward shift of the westerly in JJAS around 10° N over Africa and 20° N over South Asia. The difference between the two models is the weakening of the easterly in early summer over the Sahara region in the case of MIROC-ESM, whereas MIROC3 shows no large change in wind. This difference in early summer may lead to more moisture convergence over the Sahara according to MIROC-ESM and further enhancement of precipitation over the area.

5.3 Precipitation enhancement over the Sahara

5.3.1 Precipitation changes in 6 ka

The precipitation differences over the Sahara between MIROC-ESM and MIROC3 are further investigated. Figure 22 compares the 6 ka precipitation change from May to

CPD
8, 3277–3343, 2012

June (MJ) and from July to September (JAS) over northern Africa for the two models. The hatched area suggests that the difference between 0 ka and 6 ka precipitation is not significant at the 95 % confidence level in a t-test. The difference between the two models is most pronounced in early summer over the Sahara. MIROC-ESM simulates enhancement of precipitation over the Sahara whereas MIROC3 simulates no enhancement in MJ, while in JAS, the two models simulate a similar precipitation shift northward.

5.3.2 Ocean feedback

It is known that SST variability greatly affects the African monsoon (Rodriguez-Fonseca et al., 2011; Mohino et al., 2011; Losada et al., 2010a, b; Fontaine et al., 2010; Bader and Latif, 2003; Vizy and Cook, 2001). Therefore, the ocean SST in 6 ka is a candidate source of precipitation change. This is investigated using the MIROC3 AGCM. We performed two sets of 0 ka and 6 ka experiments. One set used climatological SSTs simulated by MIROC-ESM (M3Aesm) as the oceanic boundary condition, and the other used climatological SSTs simulated by MIROC3 (M3Amiroc3) as listed in Table 4. The reason for using the AGCM of MIROC3 is mainly its speed of integration and the associated low computational cost compared with the case for MIROC-ESM. This test does not directly give the reason for the 6 ka precipitation change simulated in MIROC-ESM but may imply the effect of the SST change on precipitation changes.

Note that the atmosphere-ocean interaction is ignored in these sensitivity experiments. The aim here is to check if a difference in the climatological SST changes in 6 ka can influence the precipitation enhancement over the Sahara. To check if the experimental setting of the sensitivity experiments can reproduce the monsoon changes in 6 ka in the original coupled experiments, the seasonal evolutions of the precipitation changes for the original fully coupled MIROC3 simulations and M3Amiroc3 are compared for the African and Asian areas (data not shown). The seasonal evolution suggests that the 6 ka precipitation changes of MIROC3 can be reproduced using M3Amiroc3 for the African area; however, there is a significant difference between

CPD
8, 3277–3343, 2012

MIROC3 and M3Amiroc3 for the Asian area, implying that short-term SST variability and/or ocean-atmosphere interaction play a role for the Asian area. Therefore, we look at only the African area in the sensitivity experiments.

The Hovmoller diagrams in Fig. 23 show weak precipitation enhancement over the Sahara in MJ in M3Aesm similar to that in MIROC-ESM whereas this enhancement is not seen in M3Amiroc3. The precipitation changes in MJ for the African area are plotted in Fig. 24 for the coupled experiments and sensitivity experiments. The AGCM sensitivity experiments show a difference in precipitation enhancement over the Sahara due to the different climatological SSTs. M3Aesm simulates enhanced precipitation over the Sahara in 6 ka whereas M3Amiroc3 simulates reduced precipitation. Significant differences between MIROC-ESM and MIROC3 and between M3Aesm and M3Amiroc3 are suggested by the nonhatched area in Fig. 24a and c. The 6 ka-to-0 ka precipitation change ratios over the Sahara desert region (20° W–30° E, 15–35° N) are +42 % for MIROC-ESM, +2 % for MIROC3, +23 % for M3Aesm, and −8 % for M3Amiroc3. This implies that differences in the SST realization between MIROC3 and MIROC-ESM can lead to precipitation differences over the Sahara.

GMPIs were also checked in the sensitivity experiments (data not shown). The GMPI over the Sahara region in 0 ka is higher for M3Amiroc3 than for M3Aesm, and M3Aesm gives a greater change in the GMPI in 6 ka than M3Amiroc3. This resembles the GMPI over the Sahara region according to MIROC-ESM and MIROC3 (Fig. 16). The slight difference in the SST pattern in 0 ka between MIROC-ESM and MIROC3 may also affect the precipitation amount in 0 ka, and it could affect the precipitation enhancement in 6 ka.

On the other hand, the global SST cooling in the 6 ka simulation using MIROC-ESM may lead to such precipitation change. To check how SST cooling affects precipitation change over the Sahara, we compared results obtained with M3Aesm and M3Aesmofs. The enhancement is significantly reduced over the Sahara in MJ when using M3Aesmofs as shown in Fig. 23. Therefore, the slightly cooled SSTs for 6 ka in

CPD
8, 3277–3343, 2012

MIROC-ESM may also play a role in the precipitation enhancement in the early summer over the Sahara.

5.3.3 Ocean variability and the influence on the African monsoon

The sensitivity experiments in the previous subsection treat the effect of the difference in climatological SSTs between models. In this subsection, we look into the correlation between the ocean variability and the African monsoon. The largest climatic variability in the atmosphere-ocean system is the El nino/Southern Oscillation (ENSO). Figure 25 illustrates nino3 indexes. The amplitudes of the 0 ka simulations using MIROC-ESM and MIROC3 are smaller than what was observed (standard deviation of 0.92 for ERA-40; Roxy et al., 2011). Therefore, although we cannot make a quantitative statement, we might be able to comment qualitatively. In 6 ka, the amplitudes of the nino3 indexes were reduced both for MIROC3 (standard deviation of 0.48 for 0 ka and 0.37 for 6 ka) and MIROC-ESM (0.39 for 0 ka and 0.38 for 6 ka). Weakening is consistent with previous modeling studies (Liu et al., 2000; Brown et al., 2008) and with what the proxy records suggest (Rodbell et al., 1999). Figures 26 (JJAS) and 27 (DJF) present the correlation between ENSO and precipitation in JJAS. These figures reveal that there seems to be no large changes in the correlation patterns for 0 ka and 6 ka. The correlation coefficients over the Sahara area are small in both models for JJAS and DJF. The correlation between North African precipitation and ENSO does not change significantly in 6 ka (Figs. 26 and 27) for both of the models. Therefore, it is not likely that the modulation of the correlation with ENSO in 6 ka affects the monsoon change significantly. However, it is still possible that the proper 0 ka ENSO representation may affect ENSO-precipitation correlations.

On the other hand, Fig. 28 plots the correlation between the year-to-year monthly values of precipitation over the northern African area and the global SST variability for 0 ka and 6 ka obtained with the two models. The correlations between the precipitation over latitudes 0–10° N and the SSTs in 0 ka and 6 ka are illustrated in Fig. 28c and f respectively for MIROC-ESM and in Fig. 28i and l respectively for MIROC3. The two

CPD
8, 3277–3343, 2012

models suggest strong positive correlation with the SST variability over the Gulf of Guinea in 0 ka. These correlations are weaker in 6 ka (Fig. 28f and l), which possibly arises from the northward shift of the precipitation belt and the associated weakened precipitation over latitudes close to Gulf of Guinea. The precipitation over dry regions (10–15° N and 15–30° N) does not have such strong correlation with the SST of nearby oceans both in 0 ka and 6 ka, as seen at tropical latitudes. Although the correlations are weak, the correlation coefficients for precipitation over semiarid latitudes (10–15° N, Fig. 28b, e, h, and k) suggest strengthened positive correlation with the Mediterranean Sea and the area of the Atlantic Ocean at roughly the same latitudes in 6 ka for both models. The same tendency is seen in the precipitation over the desert for MIROC-ESM (Fig. 28a and d), whereas the correlation is not pronounced for MIROC3 (Fig. 28g and j), which could arise from more 6 ka precipitation over the desert in MIROC-ESM. Lagged correlations were also analyzed but they revealed less correlation than Fig. 28 with similar patterns. It seems that the enhanced precipitation in 6 ka correlates more positively to the SST at nearby latitudes of the Atlantic Ocean. The circulation change in 6 ka (Fig. 17) seems to be consistent with this area of positive correlation.

5.3.4 Vegetation changes and feedback in MIROC-ESM

The LAI calculated in SEIB-DGVM is supplied to MATSIRO in MIROC-ESM. To further investigate the mechanism of vegetation change and feedback to the climate in 6 ka in MIROC-ESM simulations, we performed a set of sensitivity experiments M3Alai for 0 ka and 6 ka (Table 4) using the AGCM of MIROC3. The experiments are the same as M3Amiroc3 except that we use different LAIs obtained in 0 ka and 6 ka simulations using MIROC-ESM. The resulting 6 ka precipitation changes over northern Africa are compared with M3Amiroc3 results in Fig. 29. There is a similar level of enhanced precipitation for M3Amiroc3 and M3Alai throughout the year. This indicates that the different LAI simulated in SEIB-DGVM has little effect on the 6 ka precipitation change over the Sahara. Slightly greater enhancement of precipitation is observed around 15° N

CPD
8, 3277–3343, 2012

in early summer but not like the enhancement of precipitation over all latitudes of the Sahara.

Figure 30 plots the LAI feedback to the global temperature for JJAS and DJF. The plots show the difference in the 6–0 ka temperature change between M3Alai and M3Amiroc3. They suggest that the LAI feedback has a warming effect over high latitudes and a cooling effect mainly over desert. The cooling over desert could be associated with slightly enhanced precipitation. The most pronounced precipitation change is seen over northern Australia. As we have mentioned, there is no significant feedback to precipitation over the Sahara. The mid/high-latitude amplification of the warming in 6 ka by vegetation feedback is consistent with the results of O'ishi and Abe-Ouchi (2011), who handled the impact of vegetation coupling on MIROC using another dynamic vegetation scheme. The cooling in JJAS seen over North America suggests why there is less warming over the area in MIROC-ESM in 6 ka; therefore, vegetation feedback in Northern America may suppress warming.

6 Summary and discussion

We overviewed the Earth System Model, MIROC-ESM in comparison with a previous version of the MIROC AOGCM, namely MIROC3, in a time-slice experiment for 6 ka. One model might outperform the other in some aspects of the representation of climate change and vice versa. However, it is worth comparing the two similar models, as we know which components the models have in common or not. Analysis of the differences in climate change obtained with the two models allows exploration of the sources of difference in climate-change simulation and the ability and limitation of the models.

MIROC-ESM and MIROC3 have different atmosphere and land processes in the physical field. Since MIROC-ESM includes a full carbon cycle, it is capable of calculating atmospheric CO_2, but we do not feedback the calculated CO_2 level to the physical field in the experiments using MIROC-ESM following CMIP5/PMIP3 protocol.

CPD
8, 3277–3343, 2012

The two models simulated generally consistent changes for 6 ka. SSTs obtained with the two models are slightly lower over the tropics in 6 ka. The air temperature is higher at mid/high latitudes in the Northern Hemisphere mainly over the continents during the boreal summer, and cooler during the boreal winter. Both models simulate slightly lower net temperature changes for 6 ka but MIROC-ESM simulated a larger temperature drop than did MIROC3. This must be due to differences in the atmosphere and/or vegetation components between the two models. However, the difference is too small to judge which model presents the more appropriate change by the proxy recoreds.

The precipitation shifts northward and is enhanced over northern Africa and the area of the Asian monsoon mainly in JJAS. The 6 ka precipitation enhancement over northern Africa according to MIROC-ESM does not differ dramatically from that obtained with MIROC3, which means that newly developed components such as dynamic vegetation and improvements in the atmospheric processes do not have significant impacts on representing the 6 ka monsoon change suggested by proxy records. The small precipitation enhancement over the Sahara in MIROC-ESM in early summer could be related to the difference in the SST change between the two models and/or the representation of 0 ka SST rather than the vegetation feedback in MIROC-ESM. The influence of the 0 ka SST representation had been pointed out for precipitation enhancement in the Asian monsoon region in 6 ka by Ohgaito and Abe-Ouchi (2009). Both models simulated insufficient precipitation enhancements to maintain vegetation over the Sahara, as was the case in previous works using models that were detailed in Sect. 1.

Although the most frequent vegetation types simulated by SEIB-DGVM in MIROC-ESM reveal a northward shift of vegetation of only about one to two grids in the Sahel area in 6 ka compared with 0 ka, there are much fewer permanent desert grids over the Sahara region. There is the possibility that such sporadic vegetation is evidenced in pollen proxy records.

The effect of vegetation coupling was small in our experiments. However, it is possible that the method of coupling SEIB-DGVM to MATSIRO through LAI change affects the results of climate change simulations in the situation that the vegetation types

CPD
8, 3277–3343, 2012

significantly differ from those of present day, such as in the case of the Sahara in 6 ka. This should be addressed in future model development. However, not only improvement of the vegetation module but also, for example, improvement of the convective cloud scheme may play a role in precipitation intrusion towards the Sahara in 6 ka (Chikira et al., 2006).

Finally, it should be noted that although models are continuously developed, the representation of climate in 0 ka will never be perfect. Although MIROC models reasonably represent the 0 ka climate, further improvements such as climatological and/or variability of SST realization in MIROC-ESM and other models will allow climate-change simulations that are more robust.

Acknowledgements. NODC_WOA98 data provided by the NOAA/OAR/ESRL PSD, Boulder, Colorado, USA, from their Web site at http://www.esrl.noaa.gov/psd/.

References

Bader, J. and Latif, M.: The impact of decadal-scale Indian Ocean sea surface temperature anomalies on Sahelian rainfall and the North Atlantic Oscillation. Geophys. Res. Lett., 30, 2169–2172, 2003.

Bartlein, P. J., Harrison, S. P., Brewer, S., Connor, S., Davis, B. A. S., Gajewski, K., Guiot, J., Harrison-Prentice, T. I., Henderson, A., Peyron, O., Prentice, I. C., Scholze, M., Seppa, H., Shuman, B., Sugita, S., Thompson, R. S., Viau, A. E., Williams, J., and Wu, H. : Pollen-based continental climate reconstructions at 6 and 21 ka: a global synthesis. Clim. Dynam., 37, 775–802, 2011.

Bergengren, J. C., Thompson S. L., Pollard, D., and DeConto, R. M.: Modeling global climate-vegetation interactions in a doubled CO_2 world, Climatic Change, 50, 31–75, 2001.

Berger A.: Long-term variations of daily insolation and Quaternary climatic changes, J. Atmos. Sci., 35, 2362–2367, 1978.

Biasutti, M., Held, I. M., Sobel, A. H., and Giannini, A.: SST forcings and Sahel rainfall variability in simulations of the twentieth and twenty-first centuries, J. Climate, 21, 3471–3486, 2008.

CPD
8, 3277–3343, 2012

Bigelow, N. H., Brubaker, L. B., Edwards, M. E., Harrison, S. P., Prentice, I. C., Anderson, P. M., Andreev, A. A., Bartlein, P. J., Christensen, T. R., Cramer, W., Kaplan, J. O., Lozhkin, A. V., Matveyeva, N. V., Murray, D. F., Mcguire, A. D., Razzhivin, V. Y., Ritchie, J. C., Smith, B., Walker, D. A., Gajewski, K., Wolf, V., Holmqvist, B. H., Igarashi, Y., Kremenetskii, K., Paus, A., Pisaric, M. F. J., and Volkova, V. S.: Climate change and Arctic ecosystems: 1. Vegetation changes north of 55 degrees N between the last glacial maximum, mid-Holocene, and present, J. Geophys. Res.-Atmos., 108, 8170–8194, 2003.

Braconnot, P., Joussaume, S., Marti, O., and De Noblet, N.: Synergistic feedbacks from ocean and vegetation on the African monsoon response to mid-Holocene insolation, Geophys. Res. Lett., 26, 2481–2484, 1999.

Braconnot, P., Joussaume, S., De Noblet, N., and Ramstein, G.: Mid-holocene and Last Glacial Maximum African monsoon changes as simulated within the Paleoclimate Modelling Intercomparison Project, Global Planet. Change, 26, 51–66, 2000.

Braconnot P., Harrison, S. P., Kageyama, M., Bartlein, P. J., Masson-Dermotte, V., Abe-Ouchi, A., Otto-Bliesner, B., and Zhao, Y.: Evaluation of climate models using palaeoclimatic data, Nat. Clim. Change, 2, 417–424, doi:10.1038/nclimate1456, 2012.

Brostrom, A., Coe, M., Harrison, S. P., Gallimore, R., Kutzbach, J. E., Foley, J., Prentice, I. C., and Behling, P.: Land surface feedbacks and palaeomonsoons in northern Africa, Geophys. Res. Lett., 25, 3615–3618, 1998.

Brown, J., Collins, M., Tudhope, A. W., and Toniazzo, T.: Modelling mid-Holocene tropical climate and ENSO variability: towards constraining predictions of future change with palaeodata, Clim. Dynam., 30, 19–36, 2008.

Chikira, M., Abe-Ouchi, A., and Sumi, A.: General circulation model study on the green Sahara during the mid-Holocene: An impact of convection originating above boundary layer, J. Geophys. Res.-Atmos., 111, 21103–21121, 2006.

Claussen, M. and Gayler, V.: The greening of the Sahara during the mid-Holocene: results of an interactive atmosphere-biome model, Global Ecol. Biogeogr., 6, 369–377, 1997.

Dallmeyer, A., Claussen, M., and Otto, J.: Contribution of oceanic and vegetation feedbacks to Holocene climate change in monsoonal Asia, Clim. Past, 6, 195–218, doi:10.5194/cp-6-195-2010, 2010.

De Noblet-Ducoudre, N., Claussen, R., and Prentice, C.: Mid-Holocene greening of the Sahara: first results of the GAIM 6000 year BP Experiment with two asynchronously coupled atmosphere/biome models, Clim. Dynam., 16, 643–659, 2000.

CPD
8, 3277–3343, 2012

Doherty, R., Kutzbach, J., Foley, J., and Pollard, D.: Fully coupled climate/dynamical vegetation model simulations over Northern Africa during the mid-Holocene, Clim. Dynam., 16, 561–573, 2000.
Douville, H., Chauvin, F., and Broqua, H.: Influence of soil moisture on the Asian and African monsoons, Part I: Mean monsoon and daily precipitation, J. Climate, 14, 2381–2403, 2001.
Douville, H., Conil, S., Tyteca, S., and Voldoire, A.: Soil moisture memory and West African monsoon predictability: artefact or reality?, Clim. Dynam., 28, 723–742, 2007.
Fontaine, B., Garcia-Serrano, J., Roucou, P., Rodriguez-Fonseca, B., Losada, T., Chauvin, F., Gervois, S., Sijikumar, S., Ruti, P., and Janicot, S.: Impacts of warm and cold situations in the Mediterranean basins on the West African monsoon: observed connection patterns (1979–2006) and climate simulations, Clim. Dynam., 35, 95–114, 2010.
Ganopolski, A., Kubatzki, C., Claussen, M., Brovkin, V., and Petoukhov, V.: The influence of vegetation-atmosphere-ocean interaction on climate during the mid-Holocene, Science, 280, 1916–1919, 1998.
Harrison, S. P., Yu, G., Takahara, H., and Prentice, I. C.: Palaeovegetation – Diversity of temperate plants in east Asia, Nature, 413, 129–130, 2001.
Harrison, S. P., Kutzbach, J. E., Liu, Z., Bartlein, P. J., Otto-Bliesner, B., Muhs, D., Prentice, I. C., and Thompson, R. S.: Mid-Holocene climates of the Americas: a dynamical response to changed seasonality, Clim. Dynam., 20, 663–688, 2003.
Hewitt, C. D. and Mitchell, J. F. B.: A fully coupled GCM simulation of the climate of the mid-Holocene, Geophys. Res. Lett., 25, 361–364, 1998.
Hurrell, J. W., Hack, J. J., Shea, D., Caron, J. M. ,and Rosinski, J.: A new sea surface temperature and sea ice boundary dataset for the Community Atmosphere Model, J. Climate, 21, 5145–5153, 2008.
Joussaume, S., Taylor, K. E., Braconnot, P., Mitchell, J. F. B., Kutzbach, J. E., Harrison, S. P., Prentice, I. C., Broccoli, A. J., Abe-Ouchi, A., Bartlein, P. J., Bonfils, C., Dong, B., Guiot, J., Herterich, K., Hewitt, C. D., Jolly, D., Kim, J. W., Kislov, A., Kitoh, A., Loutre, M. F., Masson, V., Mcavaney, B., Mcfarlane, N., De Noblet, N., Peltier, W. R., Peterschmitt, J. Y., Pollard, D., Rind, D., Royer, J. F., Schlesinger, M. E., Syktus, J., Thompson, S., Valdes, P., Vettoretti, G., Webb, R. S., and Wyputta, U.: Monsoon changes for 6000 years ago: Results of 18 simulations from the Paleoclimate Modeling Intercomparison Project (PMIP), Geophys. Res. Lett., 26, 859–862, 1999.

CPD
8, 3277–3343, 2012

K-1 model developers: K-1 coupled model (MIROC) description, in: K-1 technical report, 1, edited by: Hasumi, H. and Emori, S., Center for Climate System Research, University of Tokyo, 34 pp., 2004.
Kim, H. J., Takata, K., Wang, B., Watanabe, M., Kimoto, M., Yokohata, T., and Yasunari, T.: Global Monsoon, El Nino, and Their Interannual Linkage Simulated by MIROC5 and the CMIP3 CGCMs, J. Climate, 24, 5604–5618, 2011.
Knorr, W. and Schnitzler, K. G.: Enhanced albedo feedback in North Africa from possible combined vegetation and soil-formation processes, Clim. Dynam., 26, 55–63, 2006.
Kohfeld, K. E. and Harrison, S. P.: How well can we simulate past climates? Evaluating the models using global palaeoenvironmental datasets, Quaternary Sci. Rev., 19, 321–346, 2000.
Kutzbach, J. E., Bartlein, P. J., Foley, J. A., Harrison, S. P., Hostetler, S. W., Liu, Z., Prentice, I. C., and Webb, T.: Potential role of vegetation feedback in the climate sensitivity of high-latitude regions: A case study at 6000 years BP, Global Biogeochem. Cy., 10, 727–736, 1996a.
Kutzbach, J., Bonan, G., Foley, J., and Harrison, S. P.: Vegetation and soil feedbacks on the response of the African monsoon to orbital forcing in the early to middle Holocene, Nature, 384, 623–626, 1996b.
Levis, S., Bonan, G. B., and Bonfils, C.: Soil feedback drives the mid-Holocene North African monsoon northward in fully coupled CCSM2 simulations with a dynamic vegetation model, Clim. Dynam., 23, 791–802, 2004.
Lezine, A. M., Hely, C., Grenier, C., Braconnot, P., and Krinner, G.: Sahara and Sahel vulnerability to climate changes, lessons from Holocene hydrological data, Quaternary Sci. Rev., 30, 3001–3012, 2011.
Liu, Z., Gallimore, R. G., Kutzbach, J. E., Xu, W., Golubev, Y., Behling, P., and Selin, R.: Modeling long-term climate changes with equilibrium asynchronous coupling, Clim. Dynam., 15, 325–340, 1999.
Liu, Z. Y., Kutzbach, J., and Wu, L. X.: Modeling climate shift of El Nino variability in the Holocene, Geophys. Res. Lett., 27, 2265–2268, 2000.
Liu, Z., Otto-Bliesner, B., Kutzbach, J., Li, L., and Shields, C.: Coupled climate simulation of the evolution of global monsoons in the Holocene, J. Climate, 16, 2472–2490, 2003.
Liu, Z., Harrison, S. P., Kutzbach, J., and Otto-Bliesner, B.: Global monsoons in the mid-Holocene and oceanic feedback, Clim. Dynam., 22, 157–182, 2004.

CPD
8, 3277–3343, 2012

Liu, Z., Notaro, M., and Gallimore, R.: Indirect vegetation-soil moisture feedback with application to Holocene North Africa climate, Global Change Biol., 16, 1733–1743, 2010.
Losada, T., Rodriguez-Fonseca, B., Janicot, S., Gervois, S., Chauvin, F., and Ruti, P.: A multi-model approach to the Atlantic Equatorial mode: impact on the West African monsoon, Clim. Dynam., 35, 29–43, 2010a.
Losada, T., Rodriguez-Fonseca, B., Polo, I., Janicot, S., Gervois, S., Chauvin, F., and Ruti, P.: Tropical response to the Atlantic Equatorial mode: AGCM multimodel approach, Clim. Dynam., 35, 45–52, 2010b.
Marzin, C. and Braconnot, P.: The role of the ocean feedback on Asian and African monsoon variations at 6 kyr and 9.5 kyr BP, C. R. Geosci., 341, 643–655, 2009a.
Marzin, C. and Braconnot, P.: Variations of Indian and African monsoons induced by insolation changes at 6 and 9.5 kyr BP, Clim. Dynam., 33, 215–231, 2009b.
Mohino, E., Rodriguez-Fonseca, B., Mechoso, C. R., Gervois, S., Ruti, P., and Chauvin, F: Impacts of the Tropical Pacific/Indian Oceans on the Seasonal Cycle of the West African Monsoon, J. Climate, 24, 3878–3891, 2011.
Notaro, M., Wang, Y., Liu, Z., Gallimore, R., and Levis, S.: Combined statistical and dynamical assessment of simulated vegetation-rainfall during the mid-Holocene, Global Change Biol., 14, 347–368, 2008.
O'ishi, R. and Abe-Ouchi, A.: Polar amplification in the mid-Holocene derived from dynamical vegetation change with a GCM, Geophys. Res. Lett., 38, 14702–14707, 2011.
Ohgaito, R. and Abe-Ouchi, A.: The role of ocean thermodynamics and dynamics in Asian summer monsoon changes during the mid-Holocene, Clim. Dynam., 29, 39–50, 2007.
Ohgaito, R. and Abe-Ouchi, A.: The effect of sea surface temperature bias in the PMIP2 AOGCMs on mid-Holocene Asian monsoon enhancement, Clim. Dynam., 33, 975–983, 2009.
Otto, J., Raddatz, T., Claussen, M., Brovkin, V., and Gayler, V.: Separation of atmosphere-ocean-vegetation feedbacks and synergies for mid-Holocene climate, Geophys. Res. Lett., 36, 09701–09705, 2009.
Philippon, N., Mougin, E., Jarlan, L., and Frison, P. L.: Analysis of the linkages between rainfall and land surface conditions in the West African monsoon through CMAP, ERS-WSC, and NOAA-AVHRR data, J. Geophys. Res.-Atmos., 110, 24115–24128, 2005.

CPD
8, 3277–3343, 2012

Pickett, E. J., Harrison, S. P., Hope, G., Harle, K., Dodson, J. R., Kershaw, A. P., Prentice, I. C., Backhouse, J., Colhoun, E. A., D'costa, D., Flenley, J., Grindrod, J., Haberle, S., Hassell, C., Kenyon, C., Macphail, M., Martin, H., Martin, A. H., Mckenzie, M., Newsome, J. C., Penny, D., Powell, J., Raine, J. I., Southern, W., Stevenson, J., Sutra, J. P., Thomas, I., Van Der Kaars, S., and Ward, J.: Pollen-based reconstructions of biome distributions for Australia, Southeast Asia and the Pacific (SEAPAC region) at 0, 6000 and 18,000 ^{14}C yr BP, J. Biogeogr., 31, 1381–1444, 2004.

Prentice, I. C., Jolly, D., and Participants, B.: Mid-Holocene and glacial-maximum vegetation geography of the northern continents and Africa, J. Biogeogr., 27, 507–519, 2000.

Rodbell, D. T., Seltzer, G. O., Anderson, D. M., Abbott, M. B., Enfield, D. B., and Newman, J. H.: An similar to 15,000-year record of El Nino-driven alluviation in southwestern Ecuador, Science, 283, 516–520, 1999.

Rodriguez-Fonseca, B., Janicot, S., Mohino, E., Losada, T., Bader, J., Caminade, C., Chauvin, F., Fontaine, B., Garcia-Serrano, J., Gervois, S., Joly, M., Polo, I., Ruti, P., Roucou, P., and Voldoire, A.: Interannual and decadal SST-forced responses of the West African monsoon, Atmos. Ssci. Lett., 12, 67–74, 2011.

Roxy, M., Gualdi, S., Drbohlav, H. K. L., and Navarra, A.: Seasonality in the relationship between El Nino and Indian Ocean dipole, Clim. Dynam., 37, 221–236, 2011.

Sarmiento, J. L. and Gruber, N.: Ocean Biogeochemical Dynamics, Princeton University Press, Princeton, NJ, 526 pp., 2006.

Sato, H., Itoh, A., and Kohyama, T.: SEIB-DGVM: A new dynamic global vegetation model using a spatially explicit individual-based approach, Ecol. Model., 200, 279–307, 2007.

Sekiguchi, M. and Nakajima, T.: A k-distribution-based radiation code and its computational optimization for an atmospheric general circulation model, J. Quant. Spectrosc. Ra., 109, 2779–2793, 2008.

Sueyoshi, T., Ohgaito, R., Yamamoto, A., Chikamoto, M. O., Hajima, T., Okajima, M., Yoshimori, M., O'ishi, R., Abe, M., Saito, F., Watanabe, S., Kawamiya, M., and Abe-Ouchi A.: Setup of the PMIP3 paleoclimate experiments conducted using an Earth System Model, MIROC-ESM, Geosci. Model Dev., submitted, 2012.

Takemura, T., Okamoto, H., Maruyama, Y., Numaguti, A., Higurashi, A., and Nakajima, T.: Global three-dimensional simulation of aerosol optical thickness distribution of various origins. J. Geophys. Res.-Atmos., 105, 17853–17873, 2000.

CPD
8, 3277–3343, 2012

Takemura, T., Nakajima, T., Dubovik, O., Holben, B. N., and Kinne, S.: Single-scattering albedo and radiative forcing of various aerosol species with a global three-dimensional model, J. Climate, 15, 333–352, 2002.

Takemura, T., Nozawa, T., Emori, S., Nakajima, T. Y., and Nakajima, T.: Simulation of climate response to aerosol direct and indirect effects with aerosol transport-radiation model, J. Geophys. Res.-Atmos., 110, 02202–02217, 2005.

Taylor, K. E., Stouffer, R. J., and Meehl, G. A.: A summary of the CMIP5 experimental design, available at: http://cmip-pcmdi.llnl.gov/cmip5/docs/Taylor_CMIP5_design.pdf (updates/corrections made 22 January 2011), 2009.

Texier, D., De Noblet, N., Harrison, S. P., Haxeltine, A., Jolly, D., Joussaume, S., Laarif, F., Prentice, I. C., and Tarasov, P.: Quantifying the role of biosphere-atmosphere feedbacks in climate change: coupled model simulations for 6000 years BP and comparison with palaeodata for northern Eurasia and northern Africa, Clim. Dynam., 13, 865–882, 1997.

Vizy, E. K. and Cook, K. H.: Mechanisms by which Gulf of Guinea and eastern North Atlantic sea surface temperature anomalies can influence African rainfall, J. Climate, 14, 795–821, 2001.

Voss, R. and Mikolajewicz, U.: The climate of 6000 years BP in near-equilibrium simulations with a coupled AOGCM, Geophys. Res. Lett., 28, 2213–2216, 2001.

Wang, B. and Ding, Q. H.: Changes in global monsoon precipitation over the past 56 years, Geophys. Res. Lett., 33, 06711–06714, 2006.

Wang, B., Kim, H. J., Kikuchi, K., and Kitoh, A.: Diagnostic metrics for evaluation of annual and diurnal cycles, Clim. Dynam., 37, 941–955, 2011.

Wang, B., Liu, J., Kim, H.-J., Webster, P. J., and Yim, S.-Y.: Recent change of the global monsoon precipitation (1979–2008), Clim. Dynam., doi:10.1007/s00382-011-1266-z, in press, 2011.

Wang, T., Wang, H. J., and Jiang, D. B.: Mid-Holocene East Asian summer climate as simulated by the PMIP2 models, Palaeogeogr. Palaeoecol., 288, 93–102, 2010.

Wang, Y., Notaro, M., Liu, Z., Gallimore, R., Levis, S., and Kutzbach, J. E.: Detecting vegetation-precipitation feedbacks in mid-Holocene North Africa from two climate models, Clim. Past, 4, 59–67, doi:10.5194/cp-4-59-2008, 2008.

CPD
8, 3277–3343, 2012

Watanabe, S., Hajima, T., Sudo, K., Nagashima, T., Takemura, T., Okajima, H., Nozawa, T., Kawase, H., Abe, M., Yokohata, T., Ise, T., Sato, H., Kato, E., Takata, K., Emori, S., and Kawamiya, M.: MIROC-ESM 2010: model description and basic results of CMIP5-20c3m experiments, Geosci. Model Dev., 4, 845–872, doi:10.5194/gmd-4-845-2011, 2011.

Wohlfahrt, J., Harrison, S. P., Braconnot, P., Hewitt, C. D., Kitoh, A., Mikolajewicz, U., Otto-Bliesner, B. L., and Weber, S. L.: Evaluation of coupled ocean-atmosphere simulations of the mid-Holocene using palaeovegetation data from the northern hemisphere extratropics, Clim. Dynam., 31, 871–890, 2008.

World Ocean Atlas: Tech. rep., National Oceanographic Data Center, Silver Spring, Maryland, http://www.esrl.noaa.gov/psd/, Version 2, 1998.

Xue, Y. K., Juang, H. M. H., Li, W. P., Prince, S., Defries, R., Jiao, Y., and Vasic, R.: Role of land surface processes in monsoon development: East Asia and West Africa, J. Geophys. Res.-Atmos., 109, 03105–03128, 2004.

Yang, J. L., Liu, Q. Y., Xie, S. P., Liu, Z. Y., and Wu, L. X.: Impact of the Indian Ocean SST basin mode on the Asian summer monsoon, Geophys. Res. Lett., 34, 02708–02712, 2007.

Yu, G., Chen, X., Ni, J., Cheddadi, R., Guiot, J., Han, H., Harrison, S. P., Huang, C., Ke, M., Kong, Z., Li, S., Li, W., Liew, P., Liu, G., Liu, J., Liu, Q., Liu, K. B., Prentice, I. C., Qui, W., Ren, G., Song, C., Sugita, S., Sun, X., Tang, L., Vancampo, E., Xia, Y., Xu, Q., Yan, S., Yang, X., Zhao, J., and Zheng, Z.: Palaeovegetation of China: a pollen data-based synthesis for the mid-Holocene and last glacial maximum, J. Biogeogr., 27, 635–664, 2000.

Zeng, N., Neelin, J. D., Lau, K. M., and Tucker, C. J.: Enhancement of interdecadal climate variability in the Sahel by vegetation interaction, Science, 286, 1537–1540, 1999.

Zhao, Y. and Harrison, S. P.: Mid-Holocene monsoons: a multi-model analysis of the inter-hemispheric differences in the responses to orbital forcing and ocean feedbacks, Clim. Dynam., doi:10.1007/s00382-011-1193-z, in press, 2011.

Zhao, Y., Braconnot, P., Marti, O., Harrison, S. P., Hewitt, C., Kitoh, A., Liu, Z., Mikolajewicz, U., Otto-Bliesner, B., and Weber, S. L.: A multi-model analysis of the role of the ocean on the African and Indian monsoon during the mid-Holocene, Clim. Dynam., 25, 777–800, 2005.

Zhao, Y., Braconnot, P., Harrison, S. P., Yiou, P., and Marti, O.: Simulated changes in the relationship between tropical ocean temperatures and the western African monsoon during the mid-Holocene, Clim. Dynam., 28, 533–551, 2007.

CPD
8, 3277–3343, 2012

Table 1. Model comparison of MIROC-ESM and MIROC3.

model name	MIROC-ESM	MIROC3
reference	Watanabe et al. (2011)	K-1 Model developers (2004)
model type	Earth system model	AOGCM
contributed IPCC	planned for AR5	AR4 (as miroc-medres)
resolution-atmosphere	T42L80	T42L20
resolution-ocean	~1° L44	~1° L44
top level of the atmosphere	0.003 hPa	10 hPa
Atm. Physics	improved radiation code	
Vegetation	SEIB-DGVM, MATSIRO	MATSIRO
ocean carbon cycle	yes	no
Aerosol	SPRINTARS	simplified SPRINTARS

CPD
8, 3277–3343, 2012

Table 2. Vegetation types in SEIB-DGVM.

1: Polar desert
2: Arctic/Alpine-tundra
3: tropical rain forest (wet in any month)
4: tropical rain forest (seasonally cycle of water situation)
5: tropical deciduous forest
6: temperate conifer forest
7: temperate broad-leaved evergreen forest
8: temperate deciduous forest
9: boreal evergreen forest/woodland
10: boreal deciduous forest/woodland
11: short grass land
12: tall grass land
13: moist savannas
14: dry savannas
15: xeric woodland/scrub
16: Arid shrubland/steppe
17: Desert

CPD
8, 3277–3343, 2012

Table 3. Experimental setup and experiment names for MIROC-ESM and MIROC3.

experimental setup	MIROC-ESM	MIROC3
1850 AD	0 ka	M30ka
0 ka + 6000 BP orbit and the greenhouse gases	6 ka	M36ka

CPD
8, 3277–3343, 2012

Table 4. Sensitivity experiments using the AGCM of MIROC3.

Exp. name	SST and sea ice	LAI
M3Amiroc3	MIROC3	MIROC3
M3Aesm	MIROC-ESM	MIROC3
M3Aesmofs	MIROC-ESM 6 ka SST is offset	MIROC3
M3Alai	MIROC3	MIROC-ESM

CPD
8, 3277–3343, 2012

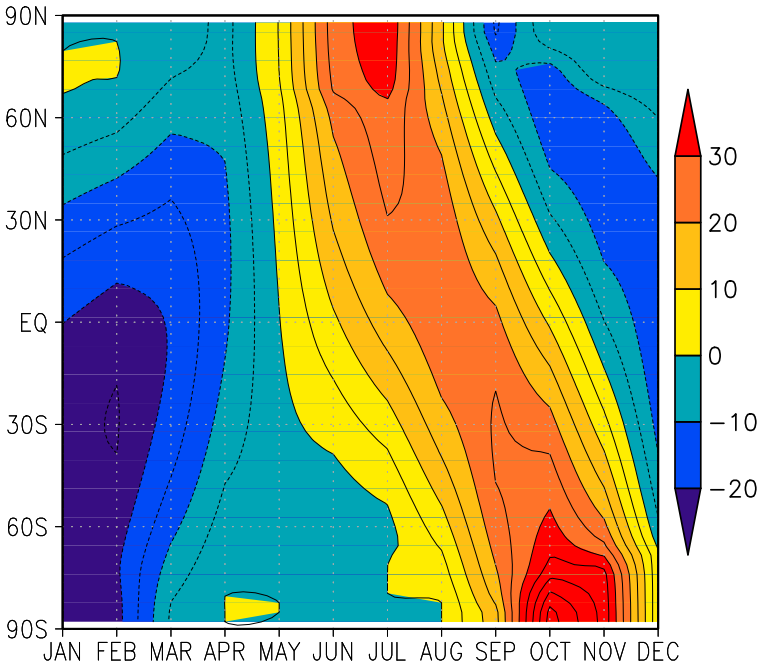

Fig. 1. Season-latitudinal difference in the solar radiation 6–0 ka ($W\,m^{-2}$).

CPD
8, 3277–3343, 2012

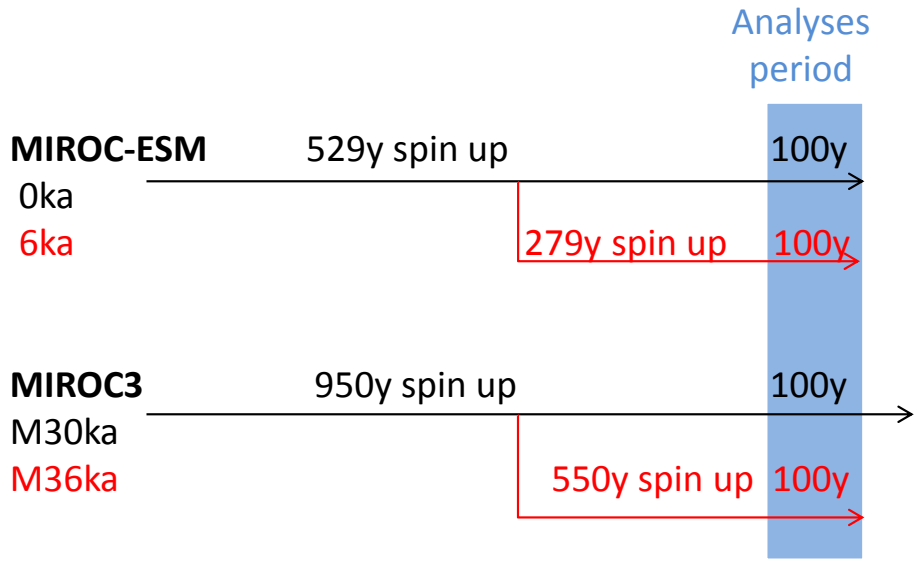

Fig. 2. Schematic illustration of the integrations in the experiments.

CPD
8, 3277–3343, 2012

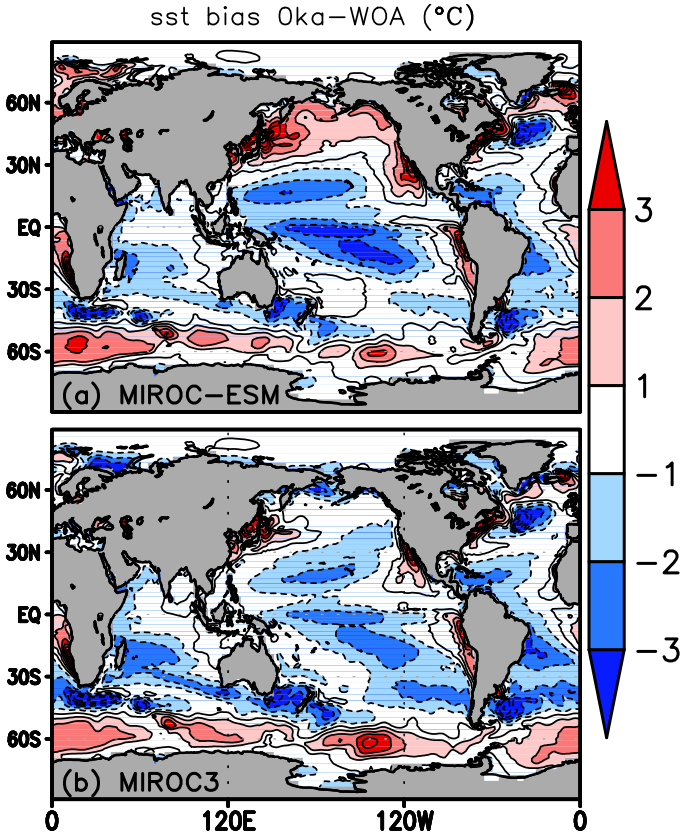

Fig. 3. 0 ka annual SST biases of **(a)** MIROC-ESM and **(b)** MIROC3 compared with the World Ocean Atlas 1998.

CPD
8, 3277–3343, 2012

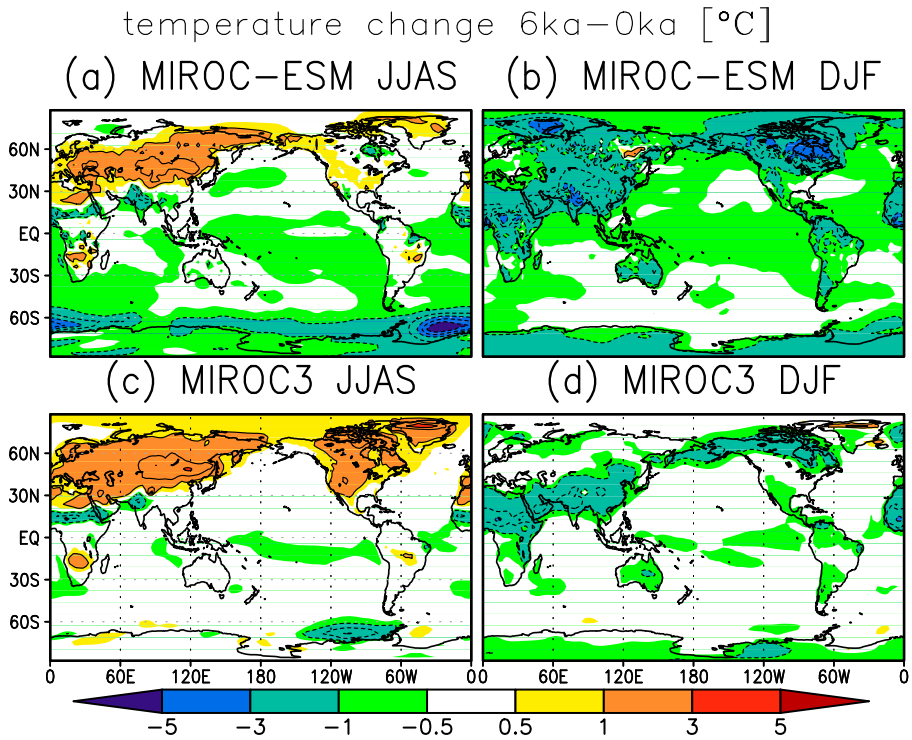

Fig. 4. 6–0 ka temperature changes at a height of 2 m (°C) in JJAS (left panels) and DJF (right panels) for MIROC-ESM (upper panels) and MIROC3 (lower panels).

CPD
8, 3277–3343, 2012

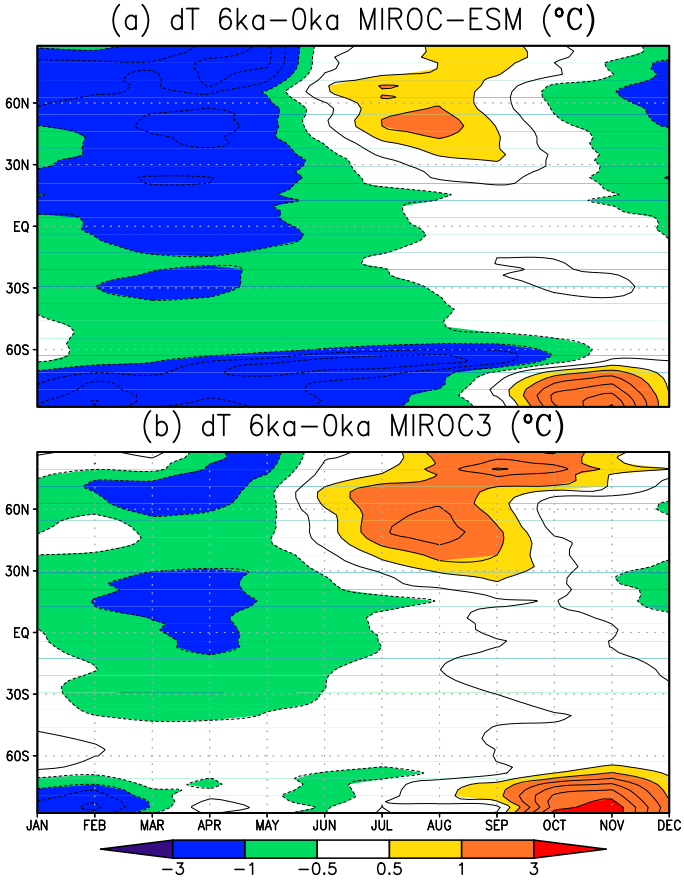

Fig. 5. 6–0 ka latitude-seasonal changes of temperature at a height of 2 m (°C) for **(a)** MIROC-ESM and **(b)** MIROC3.

CPD
8, 3277–3343, 2012

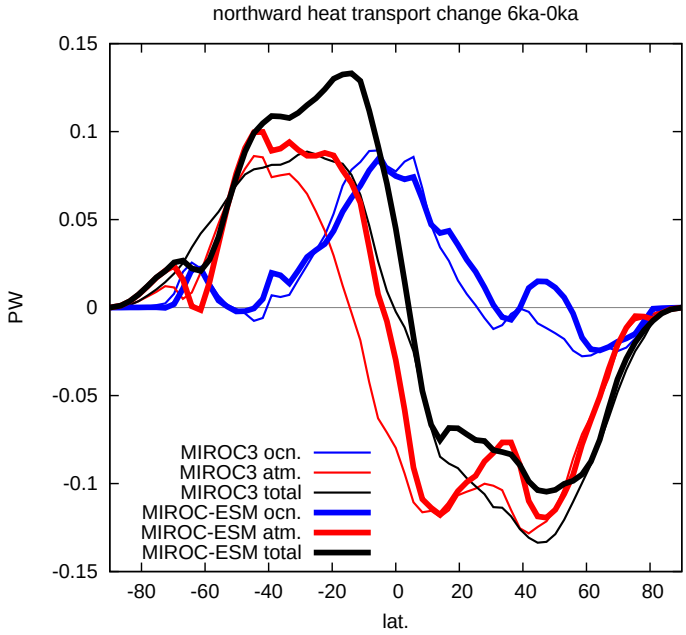

Fig. 6. 6–0 ka meridional heat transport changes by ocean (blue lines) and atmosphere (red lines) and total (black lines) for MIROC-ESM (thick lines) and MIROC3 (thin lines).

CPD
8, 3277–3343, 2012

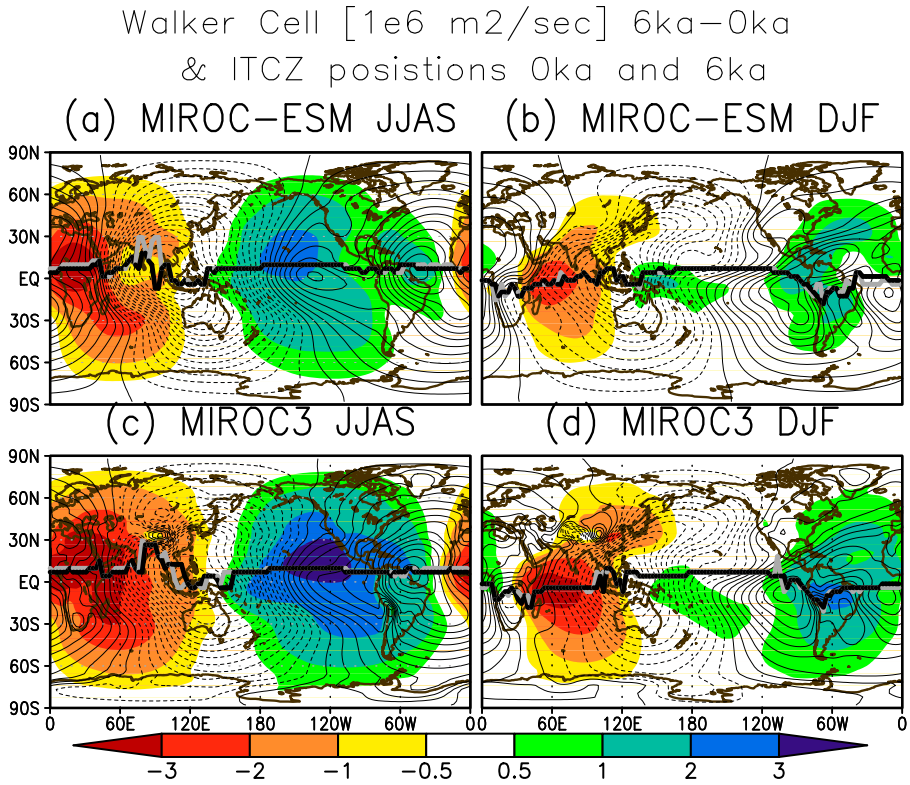

Fig. 7. Deviation from the zonal mean of the velocity potential at a pressure level of 200 hPa [10^6 m^2 s^{-1}] and the positions of the ITCZ. 6–0 ka changes (shading) in JJAS (left panels) and DJF (right panels) are plotted for MIROC-ESM (upper panels) and MIROC3 (lower panels). The thin contour lines are 0 ka values with intervals of 1×10^6 m^2 s^{-1}. The thick black and gray lines correspond to the peak latitudes of precipitation between 30° S and 30° N in 0 ka and 6 ka, respectively.

CPD
8, 3277–3343, 2012

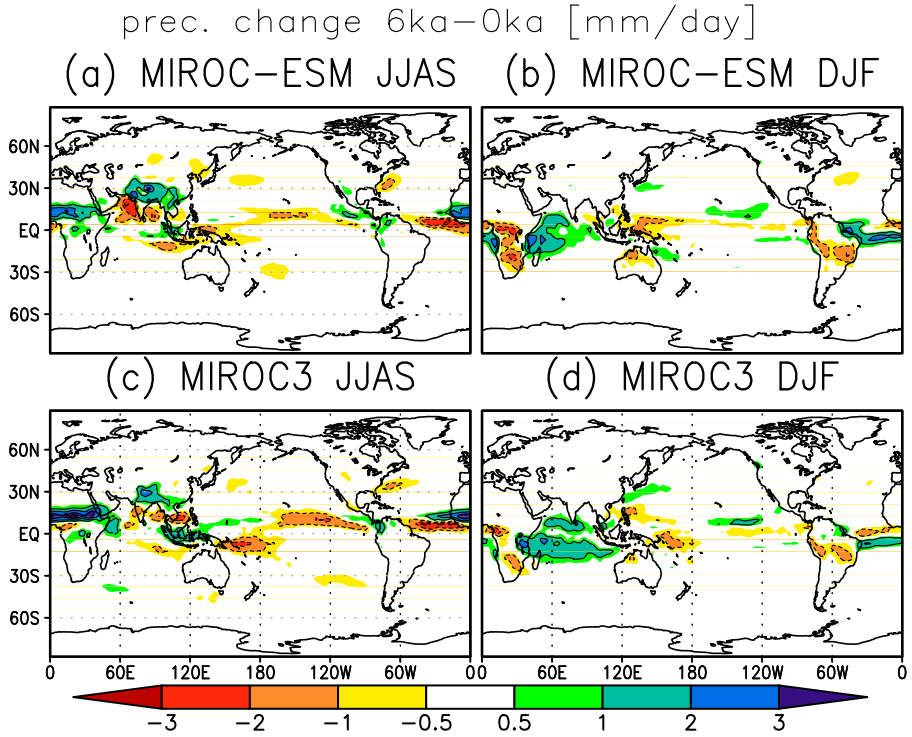

Fig. 8. The same as Fig. 4 but for precipitation changes [mm day^{-1}].

CPD
8, 3277–3343, 2012

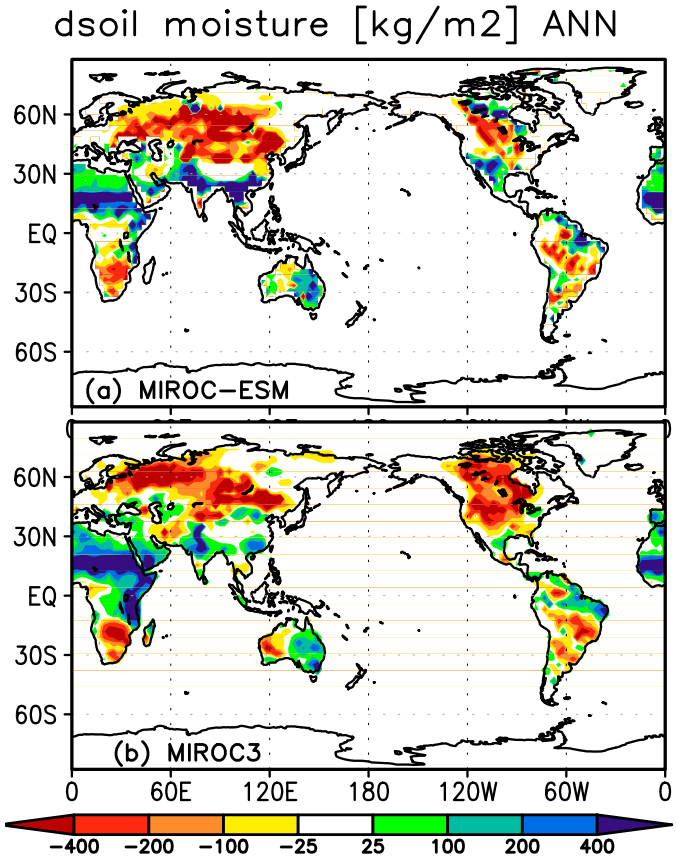

Fig. 9. 6–0 ka net soil moisture change (kg m^{-2}) for **(a)** MIROC-ESM and **(b)** MIROC3.

CPD
8, 3277–3343, 2012

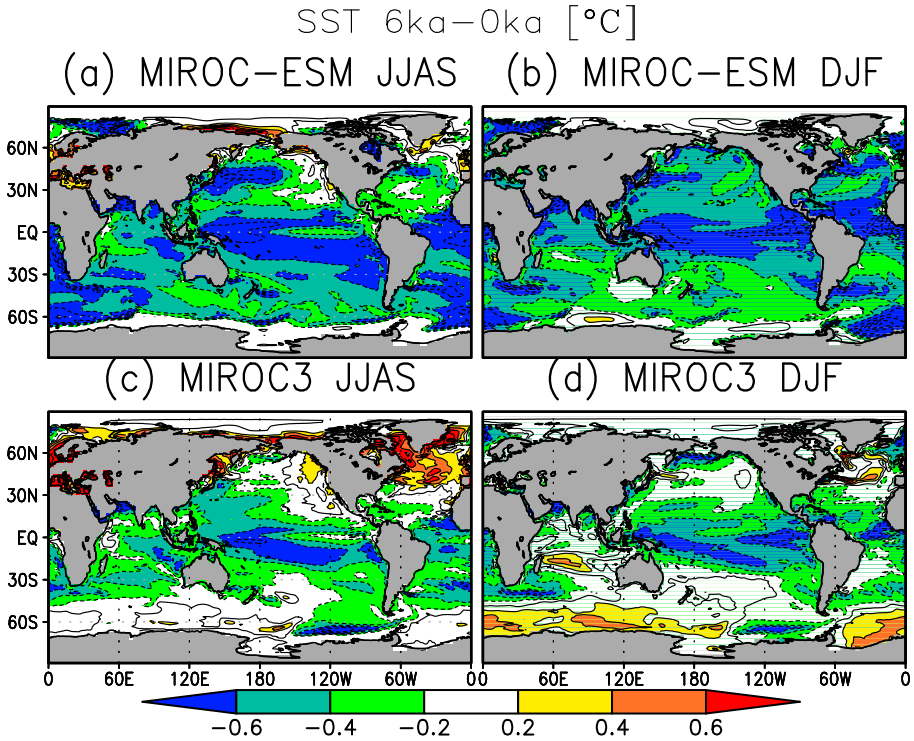

Fig. 10. The same as Fig. 4 but for the SST change (°C).

CPD
8, 3277–3343, 2012

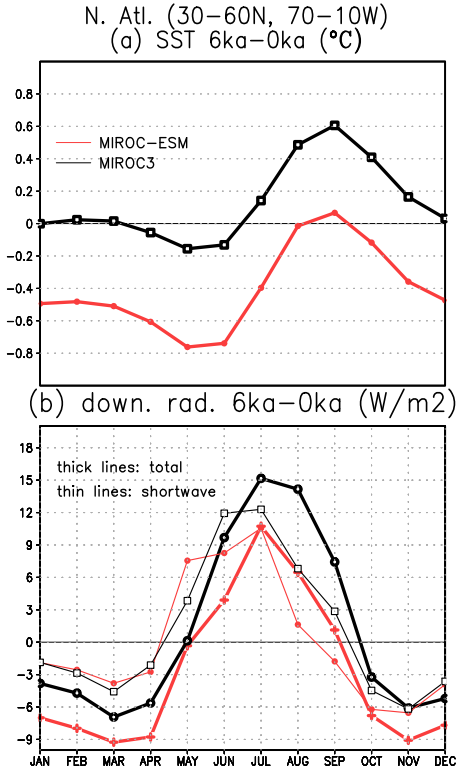

Fig. 11. (a) Seasonal evolution of the SST change (6–0 ka) over the North Atlantic region (30–60° N, 70–10° W) for MIROC-ESM (red line) and MIROC3 (black line). **(b)** The same as **(a)** but for the surface downward radiation change. The thick lines suggest total radiation changes and the thin lines suggest shortwave radiation changes.

CPD
8, 3277–3343, 2012

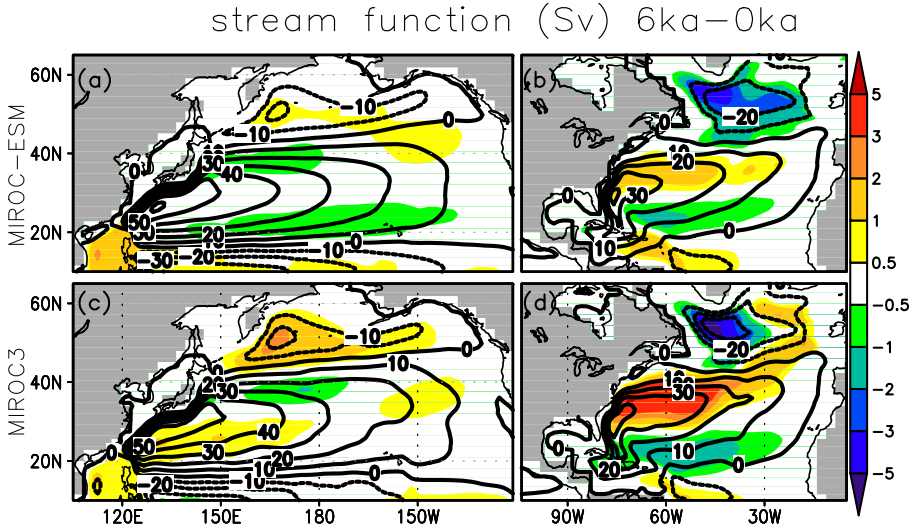

Fig. 12. Oceanic surface stream functions (contours for 0 ka) and changes in 6 ka (color) (Sv) for the Pacific and Atlantic sectors in the Northern Hemisphere obtained using **(a, b)** MIROC-ESM and **(c, d)** MIROC3.

CPD
8, 3277–3343, 2012

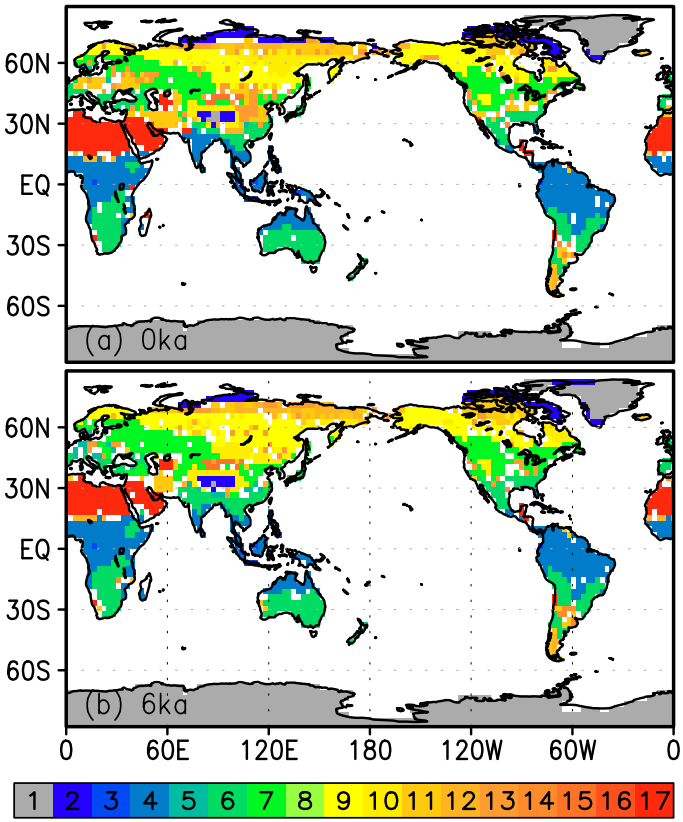

Fig. 13. Most frequent vegetation types in SEIB-DGVM for 0 ka and 6 ka by MIROC-ESM. The grids with no stable vegetation type (> 50 %) are white. Numbers in the boxes at the bottom correspond to the vegetation types listed in Table 2.

CPD
8, 3277–3343, 2012

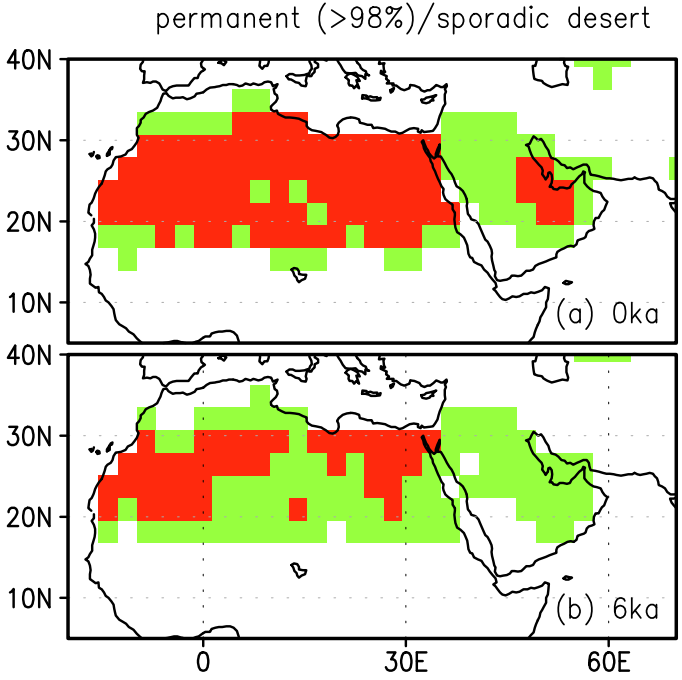

Fig. 14. Desert areas shown in Fig. 13 colored for **(a)** 0 ka and **(b)** 6 ka according to MIROC-ESM. The red grids indicate permanent desert (> 98 %), whereas green grids indicate sporadic desert.

CPD
8, 3277–3343, 2012

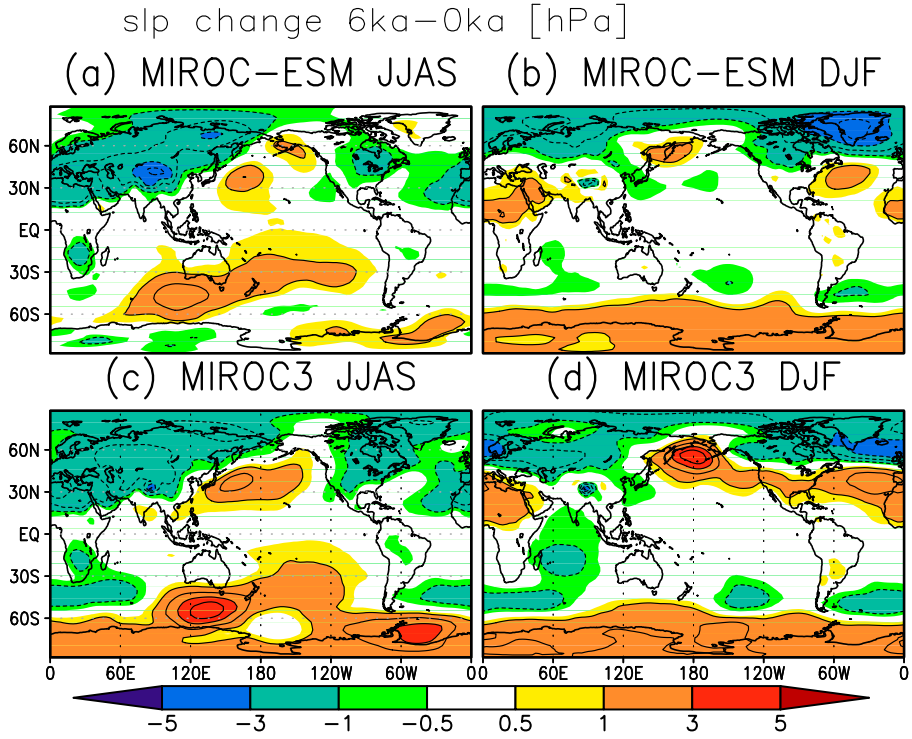

Fig. 15. Same as Fig. 4 but for sea-level pressure changes [hPa].

CPD
8, 3277–3343, 2012

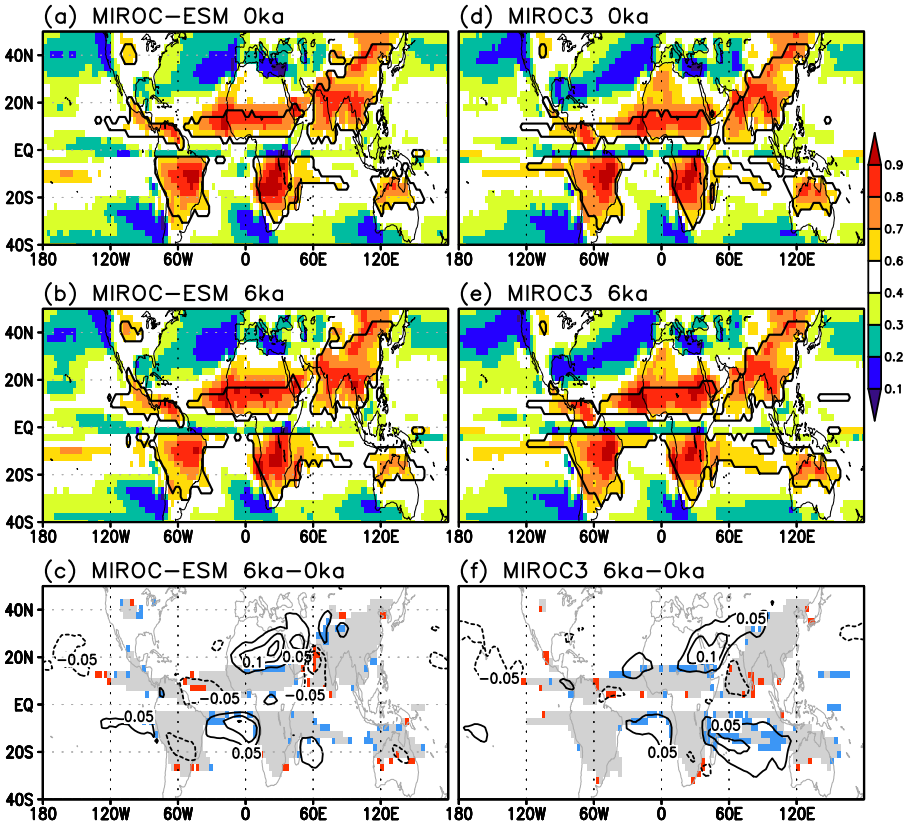

Fig. 16. Global monsoon precipitation domain (contour) and GMPI (shading) for the 0 ka (top panels) and 6 ka (middle panels) climates obtained using MIROC-ESM (left panels) and MIROC3 (right panels) analysis periods. For the change in the monsoon domain, the gray area indicates the regions identified in common, and the blue (red) area indicates the area of expansion (retreat) in the 6 ka simulations in the bottom panels. The contours give the 6–0 ka GMPI changes.

CPD
8, 3277–3343, 2012

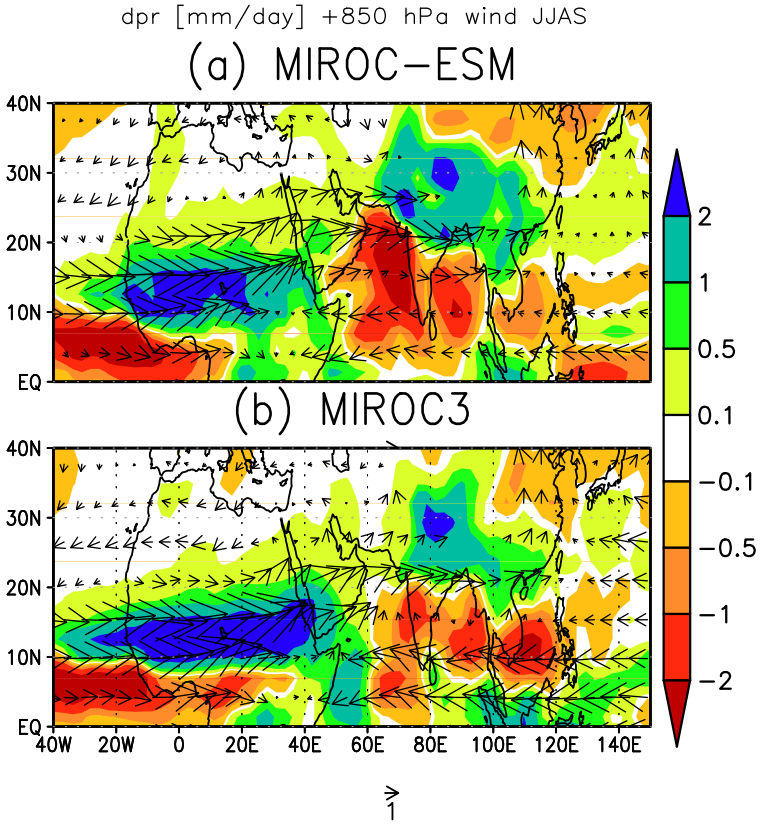

Fig. 17. 6–0 ka precipitation changes (color) and wind changes at 850 hPa (arrows) in JJAS obtained with **(a)** MIROC-ESM and **(b)** MIROC3.

CPD
8, 3277–3343, 2012

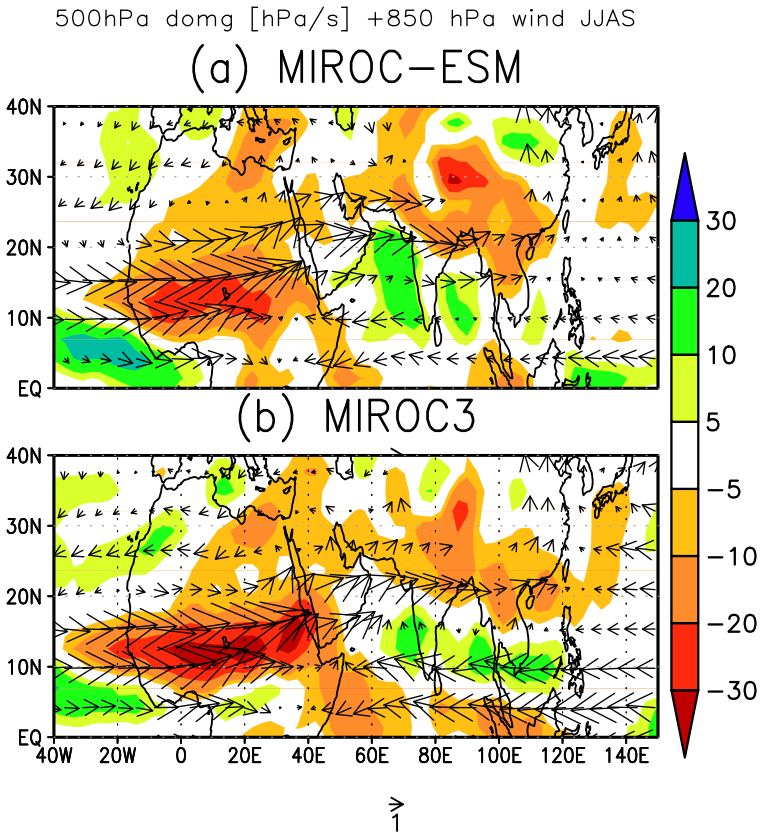

Fig. 18. 6–0 ka change in convective activity at 500 hPa (color) and wind changes at 850 hPa (arrows) in JJAS obtained with **(a)** MIROC-ESM and **(b)** MIROC3.

CPD
8, 3277–3343, 2012

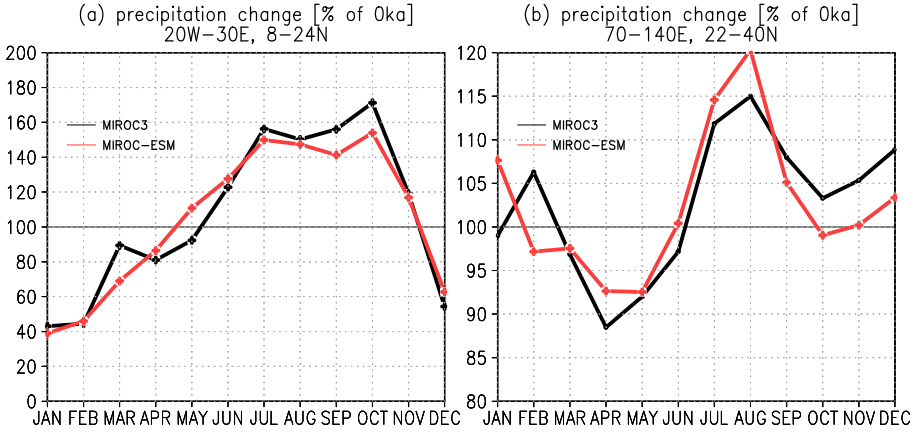

Fig. 19. 6–0 ka seasonal precipitation changes for MIROC-ESM (red lines) and MIROC3 (black lines) for the **(a)** African area (20° W–30° E, 8–24° N) and **(b)** Asian area (70–140° E, 22–40° N) as a ratio of the 0 ka precipitation amount (%).

CPD
8, 3277–3343, 2012

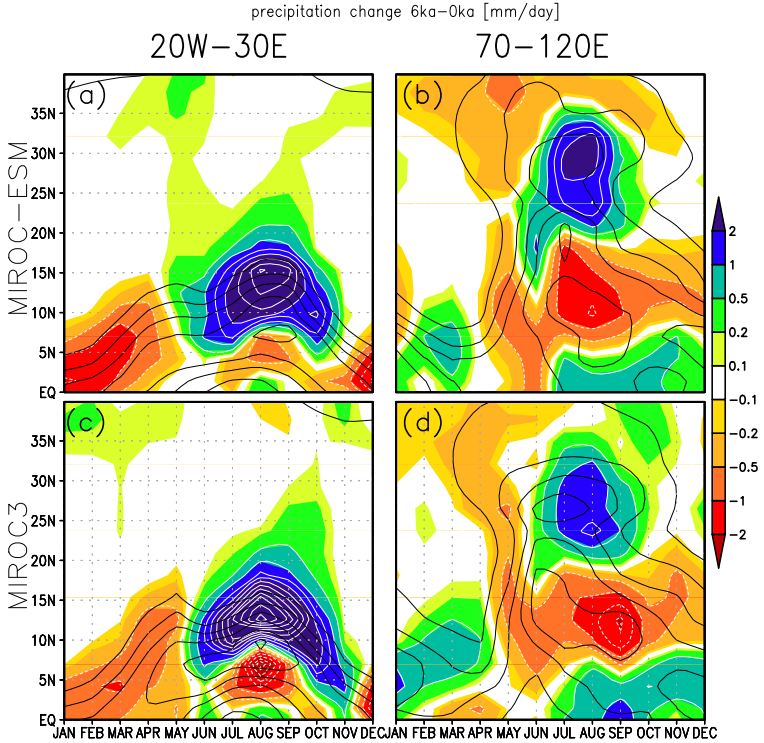

Fig. 20. Hovmoller diagrams for the northern African area (left panels) and Indian area (right panels) obtained with MIROC-ESM (upper panels) and MIROC3 (lower panels). Colors indicate the 6–0 ka precipitation change [mm day^{-1}]. Black lines are the 0 ka precipitation amount.

CPD
8, 3277–3343, 2012

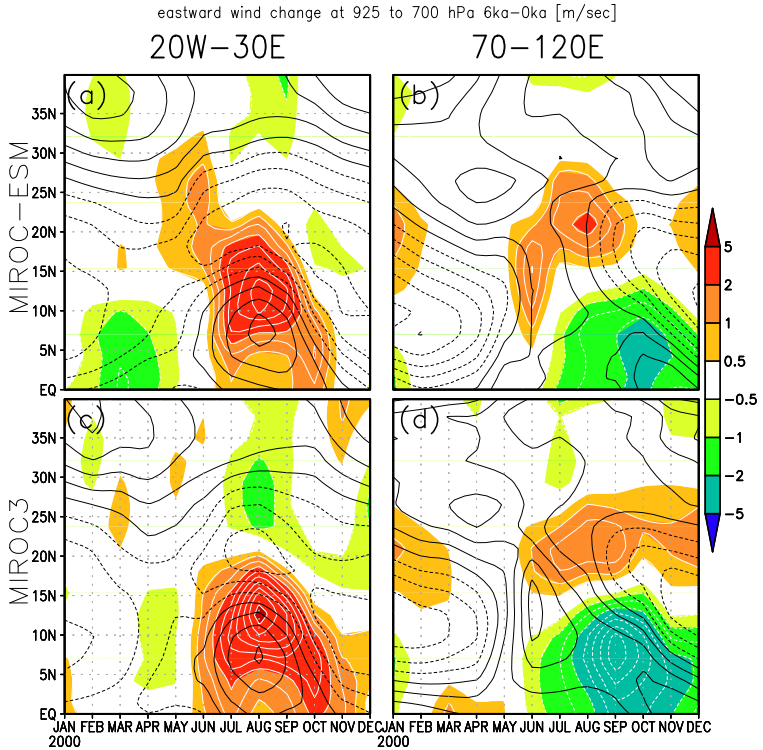

Fig. 21. Same as Fig. 20 but for the 6–0 ka zonal wind change averaged between pressure levels of 925 and 700 hPa [m s^{-1}].

CPD
8, 3277–3343, 2012

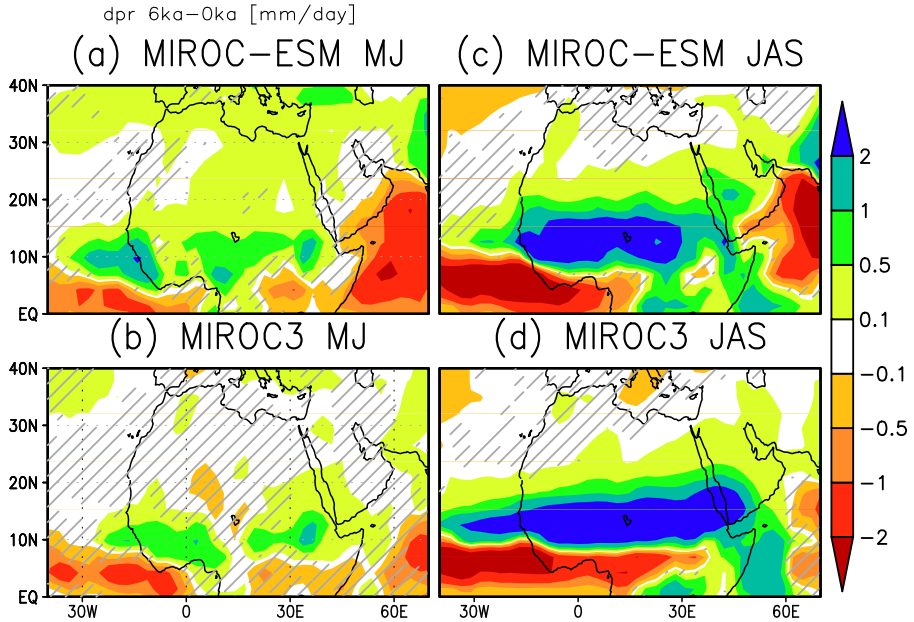

Fig. 22. 6–0 ka precipitation change for (color) [mm day^{-1}] in MJ (left panels) and JAS (right panels) obtained with MIROC-ESM (upper panels) and MIROC3 (lower panels). The hatched area is the area where the precipitation amount does not significantly differ between 0 ka and 6 ka in a t-test (95 %).

CPD
8, 3277–3343, 2012

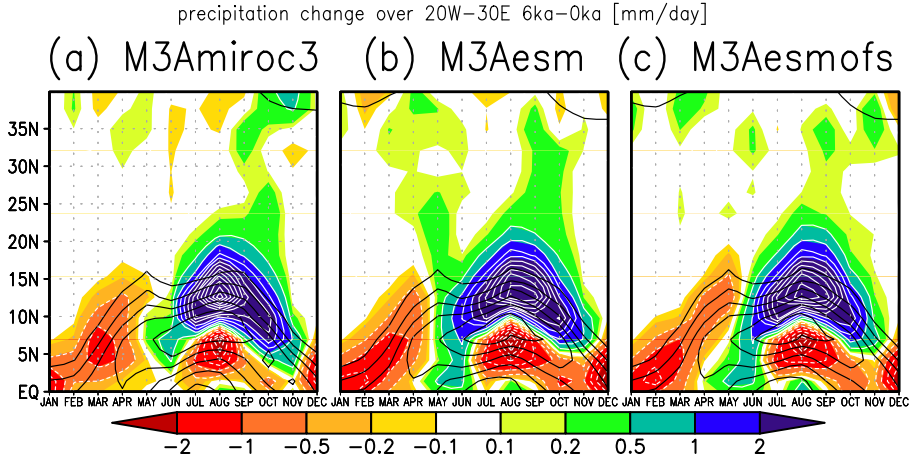

Fig. 23. Hovmoller diagrams of the precipitation change over northern Africa (20° W–30° E) for the different sensitivity experiments using the AGCM of MIROC3 **(a)** for M3Amiroc3, **(b)** for M3Aesm, **(c)** for M3Aesmofs in the same format as Fig. 20a.

CPD
8, 3277–3343, 2012

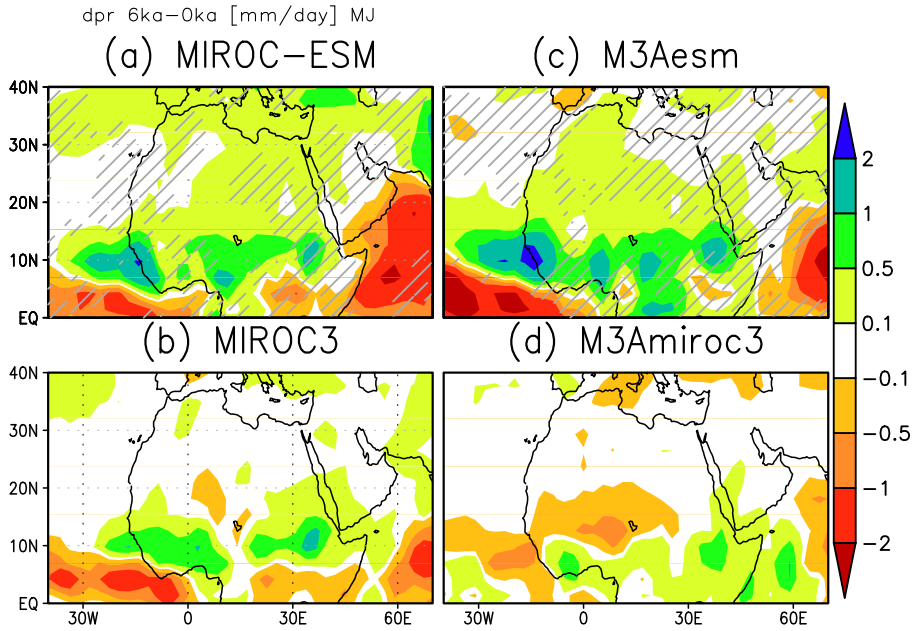

Fig. 24. 6–0 ka precipitation change over the African area in MJ [mm day^{-1}] for **(a)** MIROC-ESM, **(b)** MIROC3, **(c)** M3Aesm, and **(d)** M3Amiroc3. Hatched areas in the upper figures indicate areas where the precipitation changes in the upper panels and lower panels are insignificant in a t-test (95 %).

CPD
8, 3277–3343, 2012

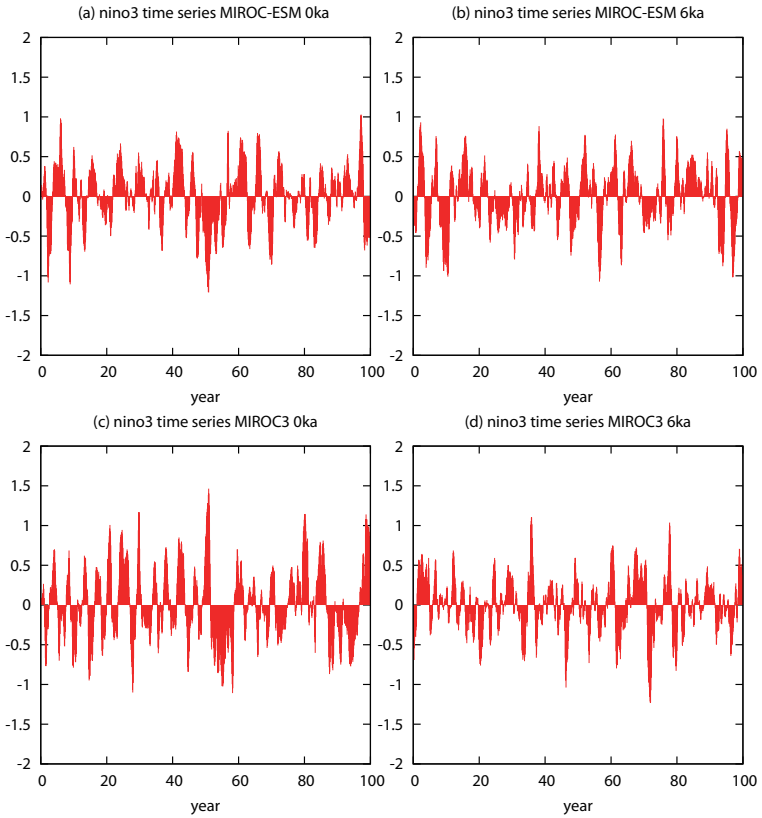

Fig. 25. Nino3 indices in 0 ka (left panels) and 6 ka (right panels) for MIROC-ESM (upper panels) and MIROC3 (lower panels).

CPD
8, 3277–3343, 2012

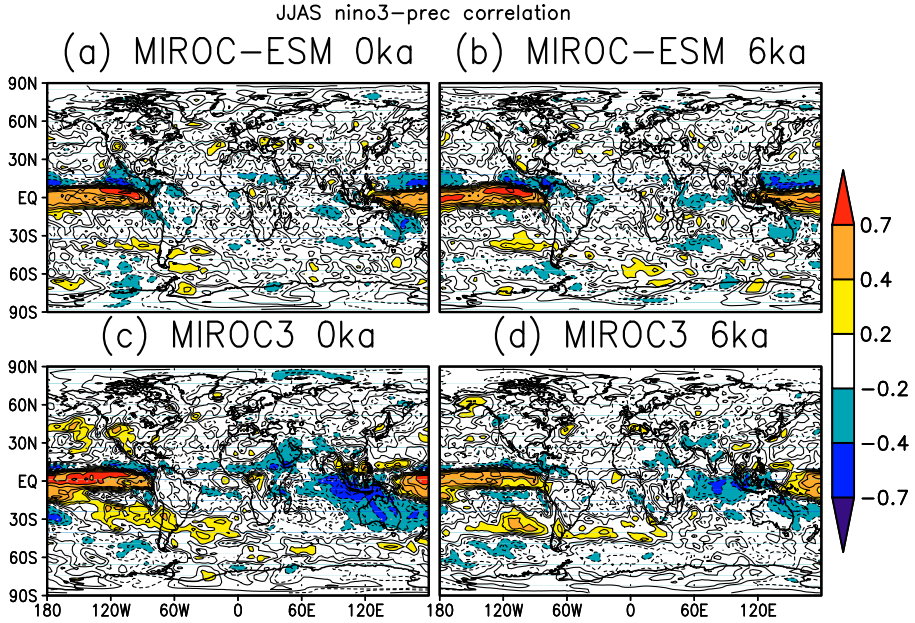

Fig. 26. Correlation coefficients of nino3-precipitation in JJAS for 0 ka (upper panels) and 6 ka (lower panels) obtained with MIROC-ESM (left panels) and MIROC3 (right panels).

CPD
8, 3277–3343, 2012

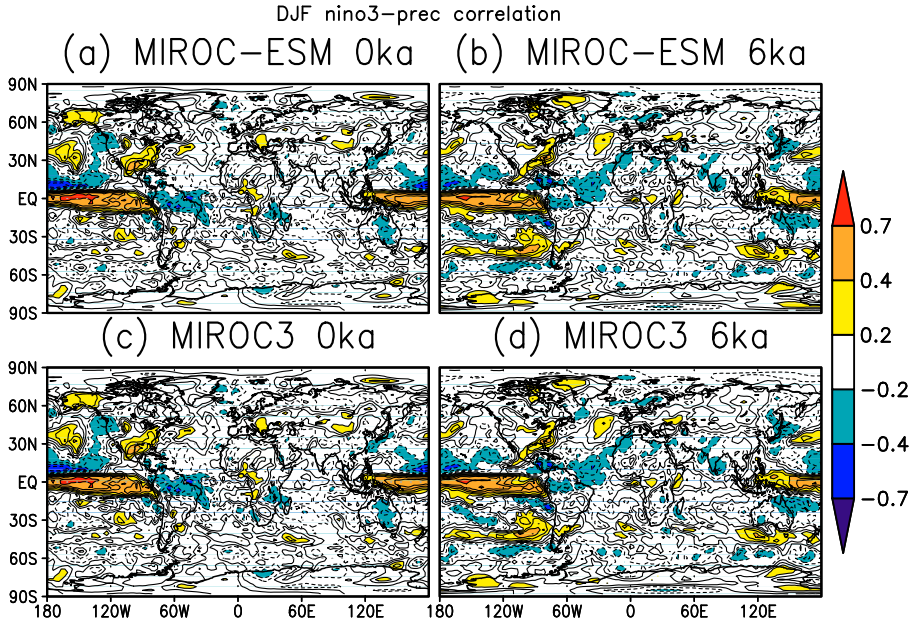

Fig. 27. Same as Fig. 26 but for DJF.

CPD
8, 3277–3343, 2012

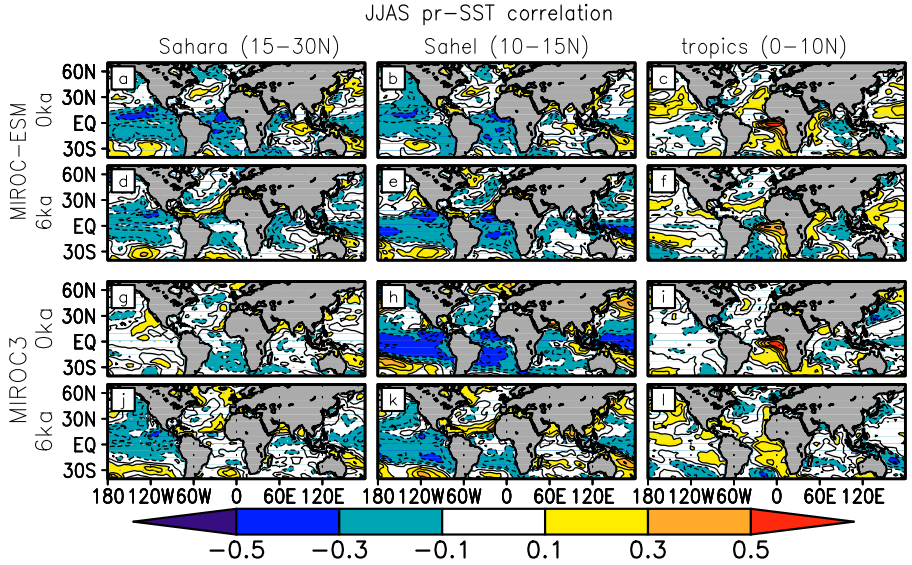

Fig. 28. Correlations between precipitation over different latitudes of the northern African (20° W–30° E) area and SSTs in JJAS for 0 ka and 6 ka obtained with MIROC-ESM for 0 ka **(a, b, c)** and 6 ka **(d, e, f)** and MIROC3 for 0 ka **(g, h, i)** and 6 ka **(j, k, l)**.

CPD
8, 3277–3343, 2012

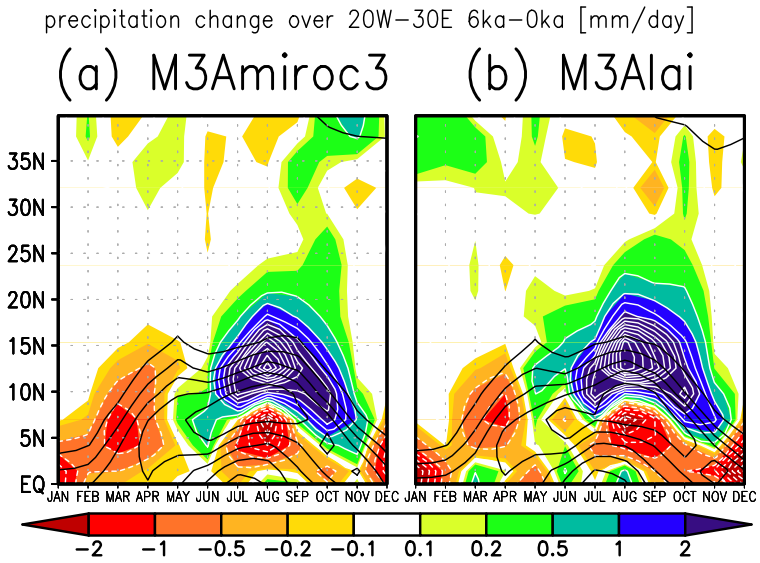

Fig. 29. Same as Fig. 23 but for **(a)** M3Amiroc3 and **(b)** M3Alai.

CPD
8, 3277–3343, 2012

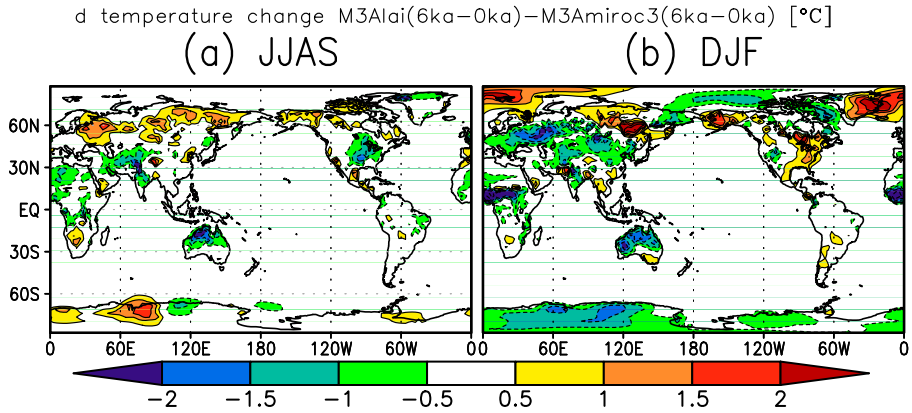

Fig. 30. Difference in the 6–0 ka temperature change between M3Alai and M3Amiroc3 (°C) for **(a)** JJAS and **(b)** DJF.

CPD
8, 3277–3343, 2012